Contents

CHAPTER ONE

The Delta Project

1.1. INTRODUCTION

This book is intended as a survey of the new European Molecular Liquids Group pilot project on a molecular liquid, carefully chosen for a *combined* study under *agreed* conditions. It is also a companion to *Molecular Dynamics* (Evans, Evans, Coffey, and Grigolini, 1982), which contains an introduction to the statistical techniques needed to study the liquid state.

1.2. THE THREE DIMENSIONS OF THE DELTA PROJECT

There were two terms: the *theoretical* and the *experimental*. We were supposed to make a theoretical hypothesis, test it experimentally, modify it and continue the cycle. However, computer simulation is a new dimension which is now being used to assist us. A new solution to the problem of understanding the liquid state of matter can now be sought within the confines of a triangle. The three corners basically refer to (1) spectral methods, (2) computer simulation, and (3) analytical theory. If generalizations can be drawn from the ideas expressed in contemporary literature on the liquid state, then it should not be surprising to find the same three themes occurring in other disciplines. This sideways method of progression has been labelled *synergetic* (Haken, 1977) and is mentioned by Professor Grigolini in Chapters 7, 8, and 9. In Chapters 3 to 6 (and in Chapter 5 with Professor Schröer), Dr. Coffey takes the formal mathematical ideas to the point where the computer is needed to solve the equation of motion numerically. Chapters 3 to 9 are therefore concerned with the theoretical corner of the triangle. However, an attempt is made in the first two chapters to show how we expect to progress with the European Molecular Liquids Group pilot project on one liquid species: dichloromethylene (methylene chloride, CH_2Cl_2; see Fig. 1.2.1). This chapter is concerned with surveying the breadth of the experimental effort involved in what has become known as the "Delta Project."

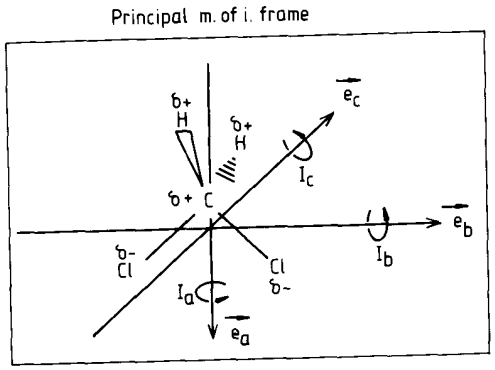

FIGURE 1.2.1. CH_2Cl_2 frame of reference, showing the unit vectors, the sign of the charge on each atom, and the principal moment-of-inertia axes.

1.3. THE PROBLEM

Within the three dimensions envisaged by the Delta Project (Evans and Yarwood, 1981), we may hope to approach the various experimental difficulties of studying the liquid state of matter with reference to the same molecular species. Wherever possible, we shall refer in this book to results already available on CH_2Cl_2. The new Delta Project results obtained by computer simulation are specially exciting. These provide us (Chapter 2) with insights into problems which have eluded precise analysis in other ways. Analytical effort to explain these new insights is underway within the Project framework and is described later.

In dealing with the liquid state, the remarks of Hildebrand (1978) provide us with a few basic criteria:

1. Do not accept concepts which are inconsistent with each other and with any *one* pertinent experimental fact. Examples of such redundant concepts are holes, cells, clusters, cages, lattices, scaled particles, fluidized vacancies, hypernetted chains, and molecules with "solidlike degrees of freedom." The computer-simulation method is less dependent on devices such as these, but it is by no means free of the necessity, for instance, of modeling the intermolecular pair potential (van der Avoird et al., 1980).

2. A theory (in this context, a model) of the liquid state that is approximately consistent with *all* the known facts under *all* the accessible thermodynamic conditions can probably be made more precise. But it must be discarded if it fails test (1).

3. The entropy of vaporization of all simple liquids (such as CH_2Cl_2) to the same concentration of vapor is the same. It is larger for associated liquids; hence simple liquids are in a state of maximum disorder and have no regular structure.

4. Simple liquids flow freely when expanded by only a few percentage points over their intrinsic volumes. There is no room for holes, lattices, or

jumps greater than a small fraction of the molecular diameter. Self-diffusion occurs because thermal motion prevents any molecule from remaining in the same spot.

5. We should define the molar volume v_t as that at which "soft" molecules begin to be sufficiently separated between collisions to acquire a fraction of their momentum in free space. At volumes smaller than v_t they are in fields of force which may not be appropriately described by pair potentials. According to Hildebrand, the role of temperature is only to determine the volume. This, though, is arguable in supercooled liquids or those under intense hydrostatic pressure. The value of v_t depends upon the capacity of a molecular species to absorb collision momentum by bending, vibrating, or rotating (Chapter 2). Pairwise interaction of model intermolecular potentials (sometimes with obscure physical attributes) is still a fundamental assumption behind computer simulation. A major effort is planned during Delta to measure quantities such as the second dielectric virial coefficient of CH_2Cl_2 (Sutter, 1972). These are required before any experimental progress can be made in dealing with the way in which molecules such as CH_2Cl_2 interact.

Having regard to these criteria, there has been a tendency to model liquid-state molecular structure and dynamics with simple ideas which do not stand up to the experimental facts now available. The theory of rotational diffusion (Debye, 1929) is an easily recognizable example of this, which, despite its elegant mathematical self-consistency, is not and *never was intended by Debye* to be a complete treatment of the problem of diffusing molecules. The theory was designed *only* to explain the absorption at *low* frequencies ($< 10^{10}$ Hz). It does not work in the far infrared range of frequencies for reasons described later. The problem of describing how molecules move about in a liquid stretches the resources of modern physics and mathematics to the limit. The methods needed to construct the various solutions to this question must be widely applicable, interdisciplinary in nature, and as simple as possible. It appears that we can only begin to obtain an objective assessment with the combined use of the three methods of spectroscopy, simulation, and theory. Within the Delta Project, there is a variety of molecular-dynamics simulation algorithms. Each of these is to be tested as thoroughly as possible and compared with the new thermodynamic and spectral data now available. We can use a much more realistic form for the intermolecular potential by using the simulation method. This cannot, however, be regarded as giving as much information about dipolar liquids as it does for other liquids. For example, by using a combination of algorithm and experimental virial data, it is possible to increase gradually the complexity of the model potential. Starting from an atom–atom Lennard-Jones basis, we may gradually add the influences of polarizability, multipole–multipole interactions, and vibrational effects, dispensing with the pairwise-additive approximation if this becomes too coarse. The problem of the reaction field (*Molecular Dynamics*, Chapter 3) is beginning to be studied using computer simulation, specially in the fields of aqueous phenomena (Berendsen et al., 1981). The algorithms written for water may

easily be adopted for CH_2Cl_2, which has the same C_{2v} symmetry. Newly developed "nonequilibrium" methods of computer simulation can be used to advantage when dealing with transport properties such as viscosity and thermal conductivity (*Molecular Dynamics*, Chapters 7, 8, and 12), and when dealing with cross-correlation functions.

The spectroscopic methods have been used in the past to look at the molecular dynamics in liquid CH_2Cl_2 in many different ways. They have never been used in unison. Further, there have been few attempts to compare the results from one technique with those gained from another. A notable exception in the literature is the work of Brier and Perry (1977), who were the first to emphasize that it is fruitless to increase the complexity of liquid-state theory without intertechnique control. This point of view was responsible, *inter alia*, for the setting up of the European Molecular Liquids Group.

After the discovery of the far-infrared absorption band of liquids (Muller and Rothschild, 1971; Chantry, 1971), it gradually became clear that the spectrum of dipolar (molecular) liquids from zero to terahertz frequencies posed a fundamental and unsolved problem of theoretical physics. The seventies have seen an intense but uncoordinated effort to develop the necessary computer software to deal with this situation. The software available now includes molecular-dynamics algorithms and algorithms for the simulation of the Liouville equation, as restyled by Mori et al. (1965, 1974, 1980). Software is also available for the numerical solution of various probability-density diffusion equations, such as Kramers's equation (Kramers, 1940). This equation often arises when modeling the liquid state. Later on, we test the ability of these algorithms to process measured spectra of CH_2Cl_2 in various environments.

There have been many attempts to use the techniques developed by Kubo, Scaife, van Kampen, Zwanzig, and others to reproduce the spectroscopic broad-band data up to and including the far infrared. Recently, a number of researchers (Evans et al., 1982; Coffey, Rybarsch and Schröer, 1982; Risken and Vollmer, 1978) have emphasized the role of nonlinearity in models of the liquid state. They have described mathematical techniques and computer software for solving the nonlinear equations of motion at the root of the problem. These investigations allow us to relate the subject of liquid-phase molecular dynamics to the broader synergetic viewpoint shared by many contemporary physicists and engineers (Haken, 1977). The nonlinear view is prevalent in those disciplines dealing with the evolution of biological processes and energy transfer on the molecular level (Kell, 1981). Some of these developments are described in Chapters 3 to 9.

In the Delta Project, however, we are primarily concerned with controlling and focusing the developments of theoretical, experimental, and computational work on carefully selected liquids at carefully chosen conditions agreed upon by each laboratory involved. The conditions for CH_2Cl_2, CH_3F, and CH_3I are fully described in the literature (Evans and Yarwood, 1981; *Molecular Dynamics*, Chapter 12).

The experimental situation prior to the Delta Project on CH_2Cl_2 has been evaluated by a literature search (a few hundred of the key papers consulted are listed in *Molecular Dynamics*, Chapter 12). In order to introduce some experimental techniques of Delta, we briefly summarize some of the main results of this search. A great deal of uncoordinated work has been carried out using infrared and Raman bandshapes and nuclear-magnetic-resonance (NMR) relaxation on several nuclei of liquid CH_2Cl_2. An intense effort was made to study this liquid with acoustic spectroscopy, but it waned without a clear outcome in the early seventies. There is more work reported on the intermolecular potential of CH_2Cl_2, a crucially important area, which suffers to date from a complete absence of data on second dielectric virial coefficients. There is also a poor appreciation of second pressure virial coefficients. In the Delta Project, we hope to rectify this situation. It should provide the available molecular-dynamics algorithms with a satisfactory (experimentally derived) parametrization of the potential-energy surface between two interacting CH_2Cl_2 molecules. The aim is to replace the contemporary use of models, such as the atom–atom Lennard-Jones-plus-charges model used in Chapter 2. This would allow the molecular dynamics algorithm to produce a complete range of theoretical spectra for further analysis. There is a small amount of modern electro-optical work available on CH_2Cl_2, but to our knowledge, only one Kerr-effect study. The polarizability of the CH_2Cl_2 molecule is known, but the anisotropy of the polarizability tensor is known much less accurately. Some estimates of the effective charges on each atom have been made, but moments higher than the molecular dipole moment $\vec{\mu}$ have not been measured.

There is therefore an imbalance of effort as reported in the literature, and this is typical of the situation in molecular liquids in general. It is evident that the molecular liquid is often chosen for technical convenience with little thought of interpretation of the resulting spectrum. Despite the number of papers, there is little attempt at coordination among techniques, even though they may all be available in the same laboratory. Prior to Delta, agreement between laboratories was apparently almost nonexistent when it came to how a particular molecular species could best be studied. (There are, however, exemplary exceptions to this.) Brier and Perry bring out these methodological weaknesses very clearly in their critical review article (1977) on the NMR relaxation and neutron-scattering work on liquid CH_2Cl_2.

The study of liquid CH_2Cl_2 under kilobars of applied pressure—an almost blank field spectroscopically—was first studied thermodynamically up to 30 kbar by Bridgman (1940). Again, when CH_2Cl_2 solutions are supercooled, the zero-to-terahertz-frequency loss and dispersion spectrum (*Molecular Dynamics*, Chapter 7) is spread over an enormous frequency range compared with the spectrum at room temperature. There are at least three distinct observable features in the supercooled condition, labeled α, β, and γ by Reid and Evans (1980). The γ feature (a small part of the overall spectrum) appears at the far-infrared frequencies. It is therefore within the range of some complementary technique such as Rayleigh light scattering. The time scale of the complete

(α, β, γ) molecular-dynamical evolution, however, approaches half the life of the universe measured in decades, posing a unique interpretative challenge. This challenge can be met to some extent by the nonlinear stochastic differential equations of the synergetic approach. The task of the experimentalists attached to Delta will be to provide a coherent set of wide-ranging spectra for comparison with the theoretical predictions about the molecular dynamics of CH_2Cl_2 in suitable supercooled solvents.

The problems of interpreting each individual spectrum are well known and are described in Chapter 6 of *Molecular Dynamics*. In CH_2Cl_2 they have also to be solved but are somewhat reduced. Particular attention has been given to the presence of collision-induced absorption, dispersion or scattering avoidance of band overlap in the infrared, etc. In some areas the challenge is greater than in others, but fundamentally we have to relate *macroscopic*, frequency-dependent observables to *molecular* motions and interactions evolving in time. This requires the intermediacy of a fluctuation–dissipation theorem based on the linear response of an appropriate molecular variable to a measuring field. The inapplicability of linear response theory to some situations of modern electro-optics (for example using pulses of intense mode-locked laser radiation to induce transient birefringence) is surmountable by the theoretical techniques described later in this volume. Development of theoretical methods for dealing with nonlinear systems is fundamental to any advance using these electro-optical techniques. This is because the transient response triggered in liquid CH_2Cl_2 by a mode-locked laser is highly nonlinear in the megawatt laser field. The same is true of the Kerr-effect transient, mentioned later in this chapter.

In Section 1.4, we consider some of the outstanding interpretative problems, several of which have been ignored in the literature (again with exceptions). Computer simulation (Chapter 2) is used as an aid in solving these wherever possible.

1.4. SPECTRAL PROPERTIES OF LIQUID DICHLOROMETHANE

1.4.1. Infrared Spectroscopy

We must emphasize the role of vibration–rotation mixing when discussing the correlation functions obtained by Fourier transformation of infrared bandshapes. A factorization of the complete rotational–vibrational autocorrelation function into its constituent vibrational and rotational parts is *not* straightforward. Perhaps the best way of proceeding is to compare the experimental correlation function (obtained, if necessary, after correction from the infrared band) with the purely orientational autocorrelation function produced by computer simulation (Chapter 2). Figure 1.4.1.1 is an illustration of this method for CH_2Cl_2 at 293 K. van Woerkom et al. (1974) have discussed this problem for CH_2Cl_2 using isotope-dilution methods over a wide temperature range in an attempt to separate predominantly vibrational contributions from

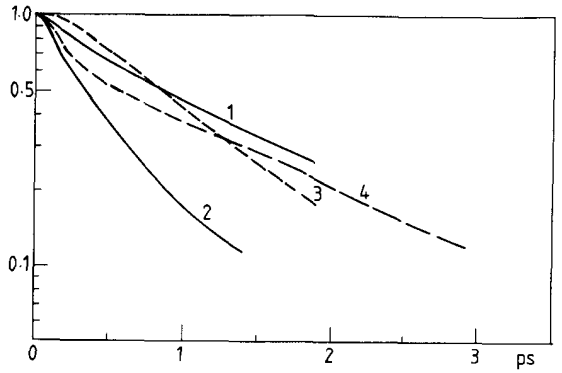

FIGURE 1.4.1.1. Curve 1: computer simulation of the orientational autocorrelation function $P_1(\vec{e}_A)$ of the dipole unit vector $\vec{e}_A$, 293 K, 1 bar. Curve 2: $P_2(\vec{e}_A)$. Curves 3 and 4: the same functions taken from a paper by van Konynenburg and Steele (1972). Curve 3 is derived from analysis of an infrared band, and curve 4 from light scattering. The match is clearly unsatisfactory and indicates the need for more work (as in Delta) to sort out the difficulties.

rotational ones. Computer simulation of intramolecular vibrational effects in the liquid environment of CH_2Cl_2 will be an important aspect of the Delta Project.

1.4.2. Raman Spectroscopy

The relevant orientational autocorrelation function for Raman spectroscopy is the second Legendre polynomial, denoted P_2 (Fig. 1.4.2.1). Raman spectra, like their infrared counterparts, are essentially rotational–vibrational in nature, and share the same factorization problems. However, both Raman and infrared spectroscopy in liquid CH_2Cl_2 are favored by the presence of proper modes with transition-moment vectors or polarizability components parallel to one of the principal moment-of-inertia axes. Therefore, the anisotropy of the molecular diffusion may be studied using different infrared and Raman bandshapes. Isotopic broadening factors are negligible compared with other sources of uncertainty in CH_2Cl_2.

Progress in the interpretation of Raman bands of liquid CH_2Cl_2 has been based, in the past, on the rather dubious process of "decoupling" the rotational relaxation from vibrational dephasing. This allows the experimentalist a method of deconvoluting the isotropic Raman spectrum. It is achieved using information derived from infrared or depolarized Raman spectra.

Unfortunately, this approach makes too many unjustifiable assumptions about $\partial^2 V/\partial q^2$, where V is the intermolecular potential energy and q a normal coordinate. It is known that coupling of vibrational and reorientational dephasing occurs when these depend on the relative orientation of two interacting molecules. Clearly this is always the case, and therefore the Delta Project will seek to use the self-consistent results from molecular-dynamics simulation.

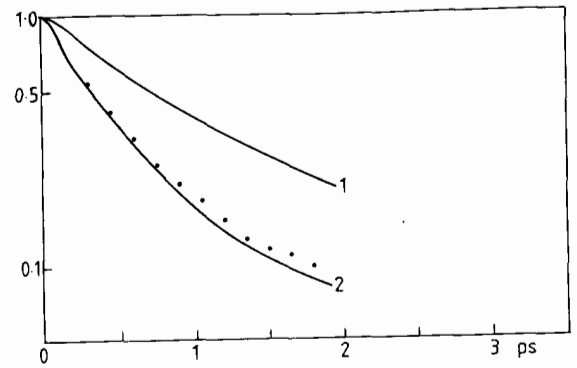

FIGURE 1.4.2.1. The anisotropy of the P_2 functions in liquid CH_2Cl_2 at 293 K, 1 bar: computer simulation. Curve 1: $P_2(\vec{e}_B)$; curve 2: $P_2(\vec{e}_A)$; points: $P_2(\vec{e}_C)$. (Refer to Fig. 1.2.1.) The simulation indicates that the diffusional rotation in CH_2Cl_2 is highly anisotropic. The anisotropy of the P_2 function has been investigated by infrared analysis in an early paper by Rothschild [*J. Chem. Phys.* **53**, 990 (1969)]. He finds correlation times $\tau(P_1(\vec{e}_A)) = 0.5$ ps, $\tau(P_1(\vec{e}_B)) = 1.1$ ps. These are far too short compared with either the dielectric relaxation times for CH_2Cl_2 (1.45 ps) or those from the computer simulation (respectively 1.2 and 3.8 ps). The infrared $\tau(P_1(\vec{e}_A))$ of Fig. 1.4.1.1, curve 3 is, on the other hand, the same as that from the computer simulation (1.2 ps). We need a coordinated effort to overcome these difficulties. The inverse of the dielectric-loss peak frequency in pure liquid CH_2Cl_2 is 1.45 ps at room temperature. This is roughly comparable to the single-molecule simulation result, 1.2 ps: the decay time of $\langle \vec{e}_A(t) \cdot \vec{e}_A(0) \rangle$. The time $\tau(P_2(\vec{e}_B)$ from light scattering ($\lesssim 1.85$ ps); see Fig. 1.4.1.1) seems to be too long; and the neutron-scattering (P_1) correlation time between the center of mass and 0.56 ps (Brier and Perry, 1977), is too short by a factor of nearly 2 compared with the computer simulation and dielectric–far-infrared results. The P_1 dielectric relaxation time for CH_2Cl_2 (liquid) is 1.45 ps.

For example, Figs. 1.4.1.1 and 1.4.2.1 illustrate P_1 and P_2 (respectively the first and second Legendre polynomial autocorrelation functions) as simulated from a model CH_2Cl_2 potential. These are compared with the available infrared and Raman data at or near the same state point. It clearly shows that vibrational decay influences the rotational motion in liquid CH_2Cl_2. Comparison of techniques is thus made more accurate through the intermediacy of the simulation algorithm. It can be made to turn (or model experimentally derived) intermolecular potentials V into a variety of spectra in a self-consistent manner.

1.4.3. Relaxation of Nuclear Magnetic Resonance

The presence of various isotopes of C, H (D), and Cl nuclei in CH_2Cl_2 is a great advantage to NMR relaxation spectroscopists when dealing with anisotropic molecular diffusion in the liquid. It is possible to use spin–spin relaxational measurements and, with a wide enough temperature span, spin–lattice relaxation. There has been much experimental work prior to Delta using this technique in liquid CH_2Cl_2. Some of this covers the necessary broad range of temperature, and in a few cases hydrostatic pressure has been applied at one or

TABLE 1.4.3.1. Comparison[a] of NMR Correlation Times and P_2 Correlation Times from a Computer Simulation of Liquid CH_2Cl_2 (293 K, 1 Bar)

Method	Vector	Correlation Time (ps)
H, intramolecular	H–H	0.53 ± 0.06
^{2}D, quadrupole relaxation	C–D	0.80 ± 0.10
^{13}C—H, dipolar	C–H	0.70 ± 0.07
^{35}Cl, quadrupole relaxation	C–Cl	1.20 ± 0.10
Computer simulation[b]	$\mathbf{e}_A$	0.50[b]
	$\mathbf{e}_B$ ($\approx$ C–Cl)	0.9[b]
	$\mathbf{e}_C$ (H–H)	0.51[b]

[a] For source references see Brier and Perry (1977).
[b] Relaxation times (e^{-1}).

two state points. However, Brier and Perry (1977) criticized this work in their review article. The fact that the NMR literature on liquid CH_2Cl_2 is inconsistent makes interpretation more uncertain. Brier and Perry were unable to obtain clear indications of the nature of anisotropic rotational diffusion in CH_2Cl_2. This was despite using a combination of NMR spectra on different nuclei, neutron scattering, and relatively straightforward analytical theory. With the help of computer simulation, this uncertainty will be reduced. Nevertheless, a coordinated effort with the various NMR techniques available is required to rectify the basic experimental differences between different literature sources. A better analytical grasp of the available NMR data is rapidly being developed by the Delta Project theoreticians. This work is described in later chapters.

Following the review article by Brier and Perry, there appeared a paper by Sandhu (1978). This was on the spin–lattice relaxation times of protons and deuterons in *oxygen-free* samples of liquid CH_2Cl_2, CD_2Cl_2, and mixtures from the melting points to the boiling point at one bar. A repetition of this work over a kilobar pressure range is planned under the Pilot Project conditions. The rotational correlation times in Sandhu's paper disagree with the values calculated by means of simple theoretical models. In Table 1.4.3.1 they are compared with a molecular-dynamics simulation of CH_2Cl_2 at two state points. Apparently, spin rotation makes no contribution to the measured NMR relaxation times in Sandhu's paper.

1.4.4. Light Scattering and Ultrasound Relaxation

Brillouin scattering and ultrasound relaxation may be used together to provide high- and lower-frequency information, respectively, on the propagation of

sound waves. This propagation is, in molecular terms, a collective phenomenon. Phonon modes in the solid become shearing modes (transverse and longitudinal) in the liquid. These can be interpreted with correlation functions built up from a long-running computer simulation. The latter can sometimes supply us with considerable supplementary information on the interaction and coupling of collective modes of molecular motion. This is one of the most interesting areas of research in the Delta Project. The results from supercooled media might well be as revealing as those already available in the related field of zero-to-terahertz spectroscopy. Here we use dielectric methods at lower frequencies than the high gigahertz range, and far-infrared spectroscopy in the terahertz range. The Brillouin peaks in scattered radiation are often observable in the gigahertz range. These have been measured in liquid CH_2Cl_2 by Caloin and Candam (1972) as a function of temperature and scattering angle. They were interpreted on a thermodynamic level by assuming a single or double relaxation of the vibrational specific heat. The study covers the necessary broad range of temperature. However, no molecular interpretation of the spectra is given. This occurs frequently in the fifty or so papers available on acoustic spectra in liquid CH_2Cl_2 (*Molecular Dynamics*, Chapter 12). In this instance there is considerable dispersion of the velocity of sound in the range 60–700 MHz, but no dispersion from 700 MHz to the gigahertz range. In the region of 0.2–3 GHz there is a scattering contribution to the absorption coefficient of sound, the acoustic dispersion producing vibrational relaxation. Hypersonic velocities of the thermal wave have been measured by Brillouin scattering spectroscopy between 4.8 and 7.2 GHz. In this range no hypersound dispersion was observed. The volume viscosity in CH_2Cl_2 is much greater than three times the shear viscosity. These are interesting spectral and molecular dynamical features hitherto uninterpreted as such. Molecular-dynamics simulation cannot yet reach down to the megahertz range for the collective correlation functions involved. However, the Delta Project has already produced interesting supplementary results on the center-of-mass autocorrelation function and, in particular, rotation–translation coupling (Bellemans et al., 1981).

The Rayleigh scattering of light by liquid dichloromethane has been investigated by van Konynenburg and Steele (1972) at one temperature and pressure. The frequency range covered is the same as that used in the technique of far-infrared spectroscopy. The two spectral techniques supplement each other in the way they regard the molecular dynamics. Both types of spectra are affected by collision-induced contributions (Evans et al., 1982). These appear to be more pronounced at short times in the light-scattering data than in the far infrared. Van Konynenburg and Steele used several recently developed models in order to interpret the long-time behavior of their correlation functions (Fig. 1.4.1.1). Infrared vibration–rotation data for liquid CH_2Cl_2 were used to supplement the Rayleigh-wing data. The former were corrected for refractive-index variability, isotope splitting, and hot refractive bands. Stokes and anti-Stokes intensities were measured to about 100-cm^{-1} shift.

1.4.5. Dielectric and Far-Infrared (Zero-to-Terahertz Frequency) Spectroscopy

Towards the end of the seventies some papers on liquid CH_2Cl_2 were written by Reid and Evans (1980), in which they attempted to take the complete (zero-to-terahertz) frequency spectrum as an entity for the purposes of interpretation. They did this by treating both the dielectric loss, $\epsilon''(\omega)$ and power absorption coefficient $\mathfrak{A}(\omega)$ (neper cm^{-1}) using one basic modeling technique. They also opened up the possibility of working with supercooled solutions of CH_2Cl_2, where the molecular dynamics are new and different. Their papers report the discovery of the γ process in dipolar molecules (illustrated in Fig. 1.4.5.1) for solutions of CH_2Cl_2 in supercooled solvents. In principle, the γ process may also be observed by other experimental techniques described in this chapter. In consequence, the preset conditions of Delta include coordinated experimental work on CH_2Cl_2 under supercooled conditions. At very low temperatures the molecular dynamical evolution (from time zero) in dilute CH_2Cl_2 solutions takes place in a continuing state of metamorphosis. Significant features of this evolution are observable over picoseconds (the γ process); it then develops into β and α motions taking place on an immensely slower time scale (Fig. 1.4.5.2). The theoretical challenge here is fundamental, because we have to produce all three (α, β, γ) distinct loss features through the intermediary of just one *molecular* orientational function. An explanation of this would be a major achievement for the theoreticians. As we have mentioned already, the conventional room-temperature zero-to-terahertz spectrum of liquid CH_2Cl_2 alone provides us with problem enough. In Fig. 1.4.5.3 we illustrate an attempt to meet this with a computer simulation algorithm (TETRAH; see also Chapter 2) of the Delta Project.

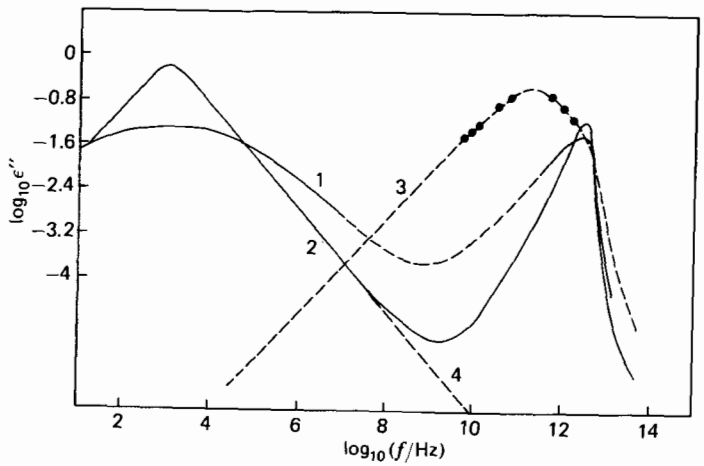

FIGURE 1.4.5.1. Complete spectrum of 10% v/v CH_2Cl_2 decalin. Curve 1: experimental curve at 110 K; curve 2: itinerant librator (two-friction version) at 110 K; curve 3: experimental points (●) on the analytical curve at 300 K; curve 4: Debye process (no description of the γ peak possible). The defect diffusion model is a combination of these processes. [Reproduced by permission from C. J. Reid and M. W. Evans, *J. Chem. Soc. Faraday Trans. II* 75, 1369 (1979).]

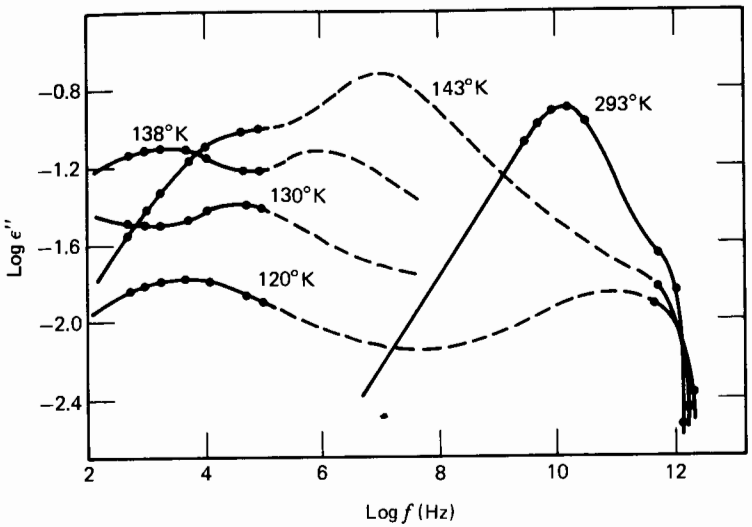

FIGURE 1.4.5.2. Multidecade loss profile of 10% v/v chlorobenzene decalin at various temperatures in the liquid, supercooled liquid, and glass (120 K). [Reproduced by permission from C. J. Reid, Ph.D. Thesis, University of Wales (1979); also C. J. Reid and M. W. Evans, *J. Chem. Phys.* **76**, 2756 (1982).]

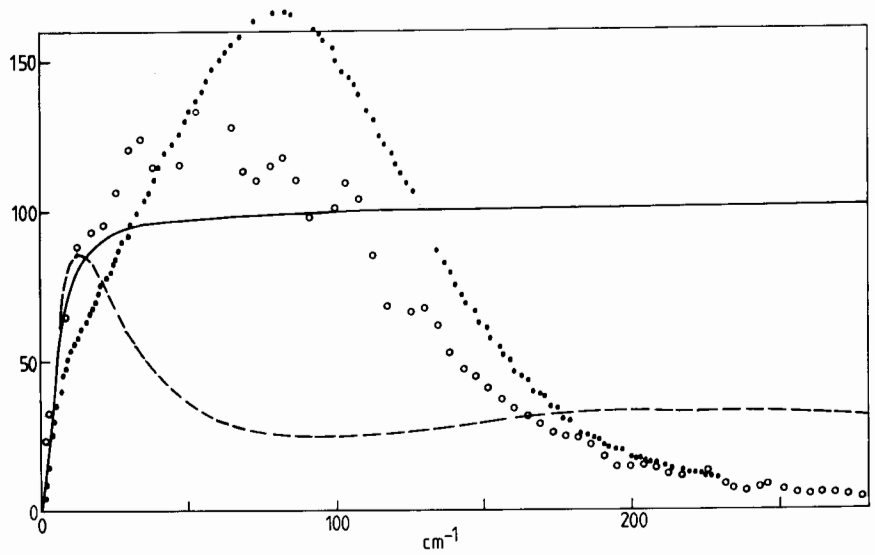

FIGURE 1.4.5.3. ○: Far-infrared power absorption of liquid CH_2Cl_2, measured with different pieces of equipment based on Michelson interferometry. ●: Computer-simulation result consisting of the numerical inverse Fourier transform of $\langle \dot{\mathbf{e}}_A(t) \cdot \dot{\mathbf{e}}_A(0) \rangle$, using the experimentally measured static permittivity ($\epsilon_s = 9.08$) to scale the absolute intensity of $\mathfrak{A}(\bar{\nu})$ (neper cm^{-1}). Solid curve: Debye's theory of rotational diffusion, which produces a plateau in the power absorption. Dashed curve: Morita's theory of asymmetric-top diffusion, which does not involve memory effects.

1.4.6. Incoherent, Inelastic Neutron Scattering

The paper by Brier and Perry (1977) describes time-of-flight spectra for liquid CH_2Cl_2 taken at the high-flux beam reactor of ILL Grenoble. Restrictions on the maximum rotor speeds available meant that the design resolution capability of this spectrometer was not achieved. As a compromise between energy-resolution and momentum-transfer requirements, the experiments were performed with an incident neutron beam energy of 1.236 meV and an energy resolution of 4%; scattering angles were 14–90°. The results (Fig. 1.4.6.1) were presented as efficiency-corrected neutron counts per second of scattered neutron flux for the given sample dimensions and orientation, normalized to unit incident flux. Multiple scattering was an essentially unsolved practical problem. The conclusions of this study illustrate the motivation behind the Delta

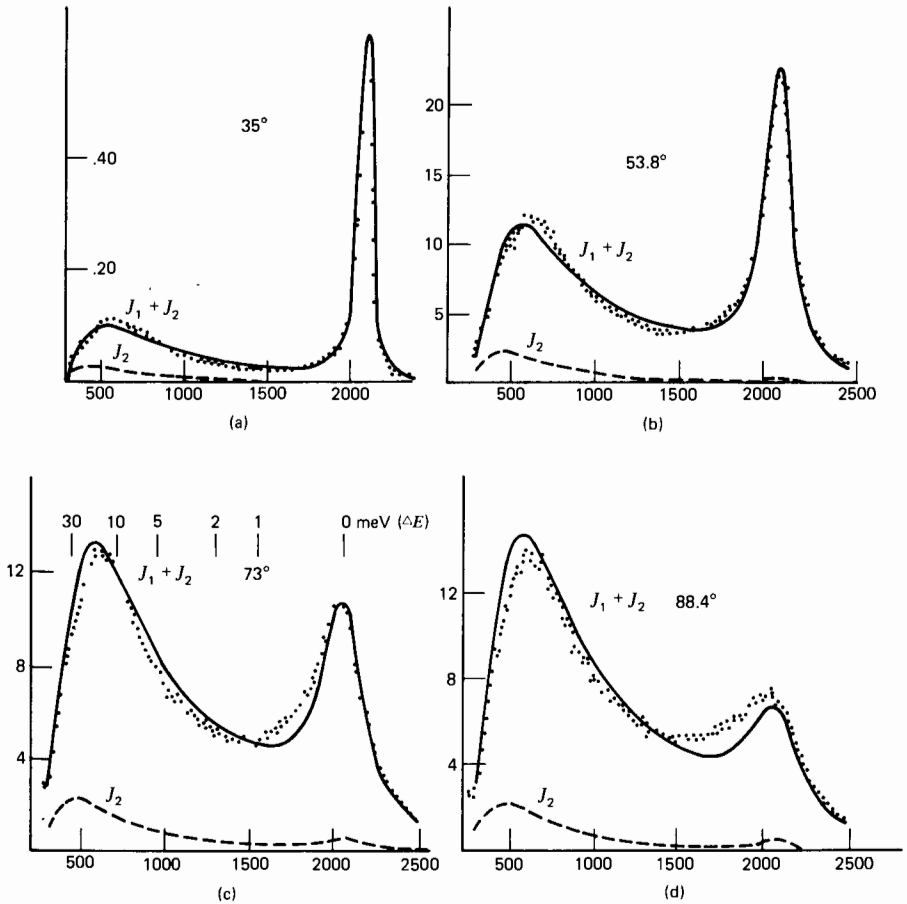

FIGURE 1.4.6.1. Experimental neutron-scattering results for CH_2Cl_2 compared with the Gordon J diffusion model. Dashed lines, experimental; solid lines, model calculations. Scattering angles are (a) 35°, (b) 53.8°, (c) 73°, and (d) 88.4°. Ordinate: count rate [10^6 neutrons s^{-1} sr^{-1} (μ s/m)$^{-1}$]. Abscissa: time of flight (μ s/m). [Reproduced by permission from Brier and Perry (1977).]

Project. We quote:

> Firstly there is the problem of assembling reliable dynamical data for a given molecular liquid. In this connection it is vital to be aware of the limitations and assumptions involved in both the measurement itself and the subsequent analysis to yield an autocorrelation function or a correlation time. Secondly there is the problem as to whether the available data are sufficiently varied and accurate to make a critical test of any model of the liquid dynamics. Here, the importance of adjusting reported measurements to common conditions, particularly temperature, and retaining realistic uncertainty limits is supreme. Thirdly, there is the general problem of the lack of theoretical models for the case of non-isotropic angular motion.

Recent progress on the third problem is described in Chapters 4 to 9. With sufficient experimental effort, the resolution of the first and second problems mentioned by Brier and Perry will be completed.

1.4.7. Vibrational-Population Lifetime of Liquid CH_2Cl_2

A paper by Laubereau et al. (1978) is available on C—H stretching modes in liquid CH_2Cl_2 excited by picosecond pulses of infrared laser radiation. The excess excited-state vibrational population is monitored by anti-Stokes scattering of subsequent ultrashort (subnanosecond) probe pulses. The observed time constants vary between 1 and 2 ps, depending on the individual molecules. Theoretical calculations of its immediate environment show that rotational coupling, Fermi resonance, Coriolis coupling, and resonance energy transfer can strongly affect the vibrational-population lifetime. The results for CH_2Cl_2 are such that the anti-Stokes scattering signal decays rapidly at first, but slows considerably after 40 ± 10 ps. This is the pattern at several different thermodynamic-state points using infrared laser radiation at 2985 and 3005 cm^{-1}. Both the ν_1 and ν_6 C—H stretching modes were excited using pulses of bandwidth $\Delta\bar{\nu} = 30\ cm^{-1}$. The initial rapid decay of the measuring signal is explained on the grounds of the fast transfer between the neighboring C—H stretching modes. The longer relaxation time is for transition to overtones and combination modes of the molecule.

1.4.8. High-Field-Induced Birefringence

With the availability of very powerful monochromatic laser fields, the transient induction of birefringence in liquid CH_2Cl_2 is a potential source of new information on molecular dynamics. Birefringence may be induced using electric and magnetic as well as electromagnetic (laser) fields, and the process may be simulated (Evans, 1982) on a computer (Fig. 1.4.8.1). Examples of some techniques involved are:

1. *High-Field Dielectric Spectroscopy.* To date, this consists essentially of inducing birefringence with a pulsed electric field of up to $10^5\ V\ cm^{-1}$. The rise

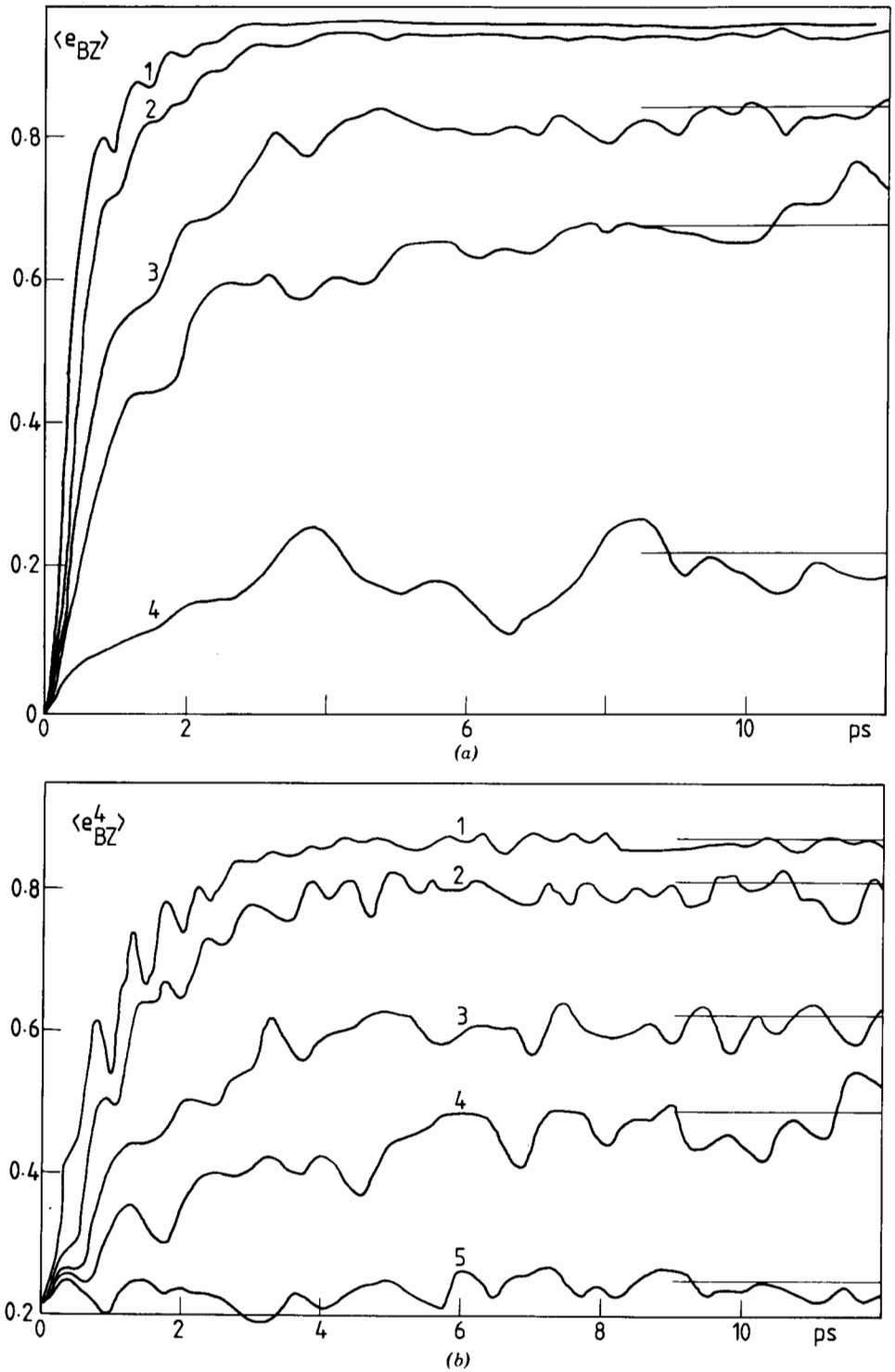

FIGURE 1.4.8.1. Top to bottom: variation of rise transient [(a) $\langle e_{BZ}\rangle$; (b) $\langle e^4_{BZ}\rangle$; (c) $\langle e^2_{BZ}\rangle$] as applied electric field decreases.

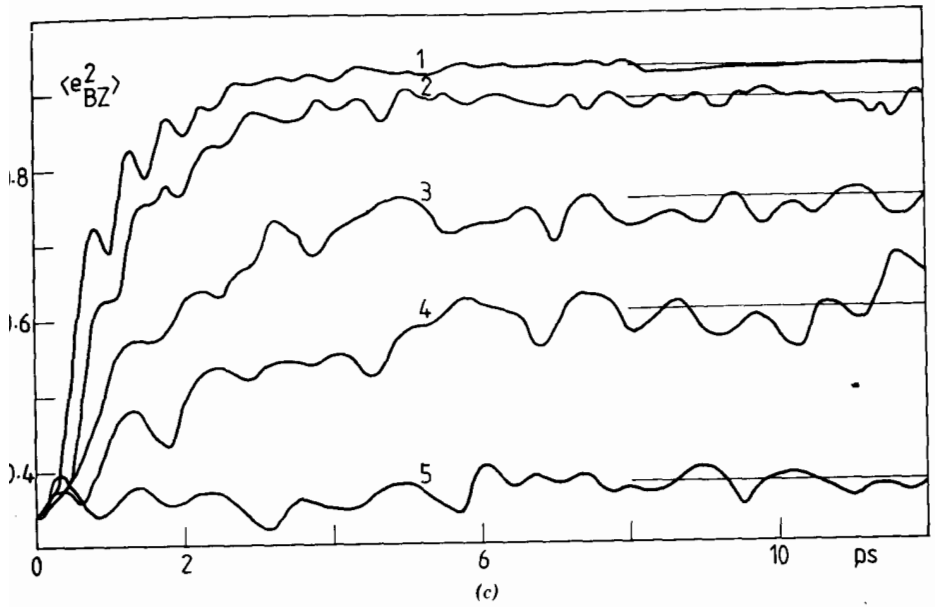

(c)

FIGURE 1.4.8.1. *Continued*

and fall transients are monitored with a measuring electric field (electrodes). The inducing field could also be a magnetic or a laser field. The birefringence is therefore expressed in terms of the dielectric permittivity and loss. If the electric field strength ($\vec{E}$) inducing the birefringence is increased indefinitely, the probability distribution function underlying the molecular motion becomes nonlinear in $\vec{E}$. As a consequence the usual linear-response theory is no longer valid. The fluctuation–dissipation theorem cannot be used to relate the macroscopically observable spectral features (rise transients) to macroscopic autocorrelation functions of the molecular motion. The analysis of the spectral data in the presence of *arbitrarily strong* driving fields is described later.

2. *Dynamic Kerr Effect* (Böttcher and Bordewijk, 1979). This is very similar to technique 1 insofar as it consists essentially of the induction of birefringence by an intense electric field applied to liquid CH_2Cl_2 as a pulse. Information may be obtained about molecular motion from the shape and duration of the rise and fall transients of induced birefringence, depending on the length of this pulse (or series of pulses). It is possible, in principle, to study the second Legendre-polynomial correlation function of the molecular reorientational process instead of the first, as in technique 1. This can be done by monitoring the latter with a weak polarized laser field. Otherwise techniques 1 and 2 share the same interpretative need for nonlinear response theory. Computer simulation can be used as an interpretative aid for any strength and any type of inducing field. This is because we can extract directly the autocorrelation functions of interest (Evans, 1982).

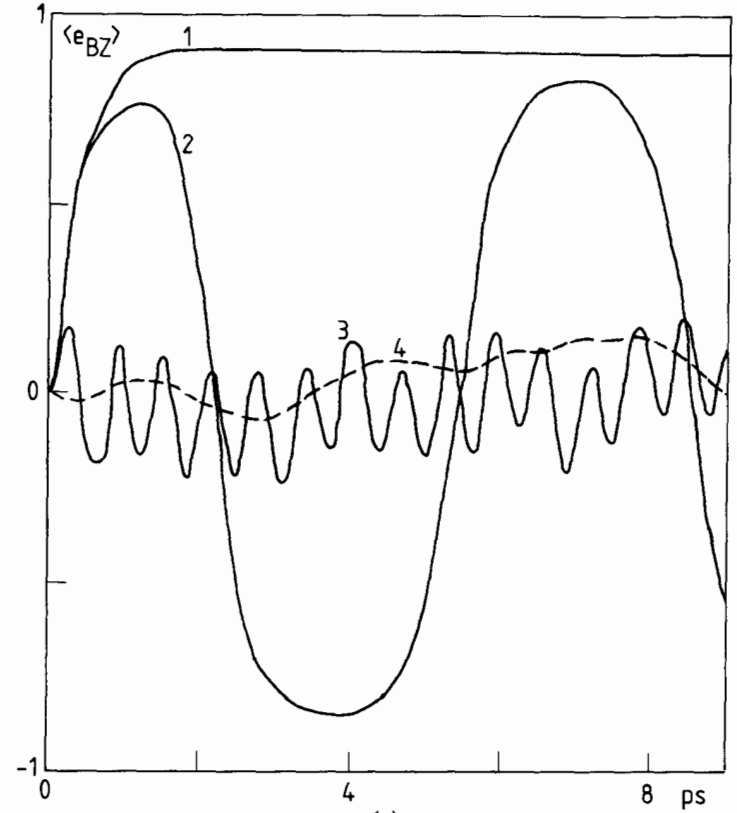

(a)

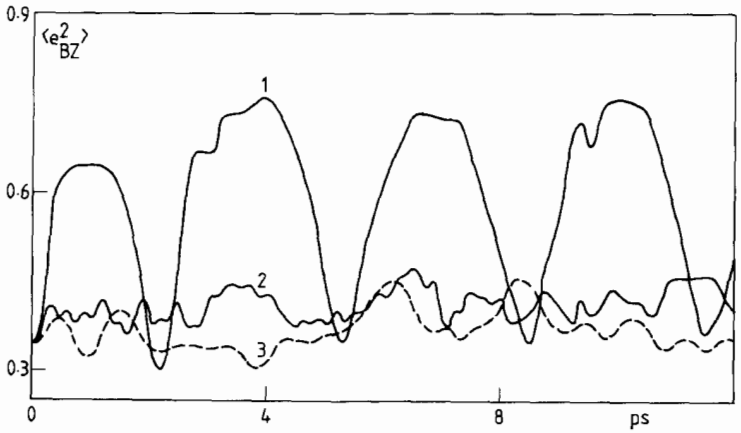

(b)

FIGURE 1.4.8.2. Rise transient $\langle e_{BZ} \rangle$ (curves 1–4) following an intense applied oscillatory field of increasing frequency; (b) Curves 1–3: increasing frequency.

Both techniques have the disadvantage that it is technically difficult to produce a pulsed electric field less than nanoseconds in duration. In the Delta Project we shall explore two ways of overcoming this by using techniques 3 and 4 below.

3. *Far-Infrared Birefringence.* The idea is simply to study the effect of an external driving field (electric, magnetic, or electromagnetic mode-locked laser) on the refractive index of liquid CH_2Cl_2 in the far infrared range of frequencies. Here, the molecular dynamics manifest themselves in an interesting way. The change in the refractive index will be monitored at spot frequencies throughout this terahertz range of frequencies (picosecond and subnanosecond time scales) with a tunable far-infrared measuring laser. Alternatively, we can use a bank of carcinotrons. The enormous (megawatt) power available in modern mode-locked lasers will induce a measurable birefringence of the refractive index in the far infrared. The results will be analysed during the Delta project, using a combination of theory and computer simulation. Far-infrared birefringence may also be induced with an alternating or pulsed electric field, whose period is not important, since we are not, in this case, dealing with transients.

4. *Picosecond Transients Induced by Laser Radiation.* This technique has been developed for measurements of birefringence transients on the picosecond or nanosecond time scale. It is similar to techniques 1 and 2. The effects of using intense laser radiation in this way have been treated by Evans (1982) using computer simulation (Fig. 1.4.8.2).

These, then, are four of the techniques being used on liquid CH_2Cl_2 under pre-agreed conditions of temperature and hydrostatic pressure. This will result in the first coordinated effort at testing out the newly available predictions of computer simulation of liquid CH_2Cl_2, discussed in the following chapter.

APPENDIX: THE FIRST EXPERIMENTAL DATA FROM THE DELTA PROJECT*

In this appendix we report the refractive indices (n_0) and dielectric permittivity (ϵ) of liquid dichloromethane. The refractive indices have been obtained over the temperature range 283–312 K using an Abbé refractometer ($\Delta n_0/n_0 = 0.1\%$). The dielectric permittivity ϵ has been measured at the EMLG pilot-project state points 223 and 312 K, at 1 bar, at the two frequencies of 9.62 and 26.62 GHz, using a method similar to that described by Finsy and van Loon [*Rev. Sci Instrum.* **44**, 409 (1973)]. The uncertainty limits are

*Forwarded by Dr. Jozeph Makosz and Professor E. Kluk, Institute of Physics, Silesian University, Universytecka 4, 40-007 Katowice, Poland.

$\Delta\epsilon'/\epsilon' = 2\%$, $\Delta\epsilon''/\epsilon'' = 3\%$. The static dielectric permittivity CP was determined from capacitance measurements at 1 kHz using bridge methods.

The Experimental Values

T (K)	312	303	293	283	273	263	253	243	233	223
n_0	1.412	1.418	1.425	1.432	1.438	1.445	1.452	1.459	1.465	1.472
ϵ_s(1 kHz)	8.25	8.62	9.03	9.45	9.93	10.38	10.80	11.23	11.68	12.15
ϵ' (9.62 GHz)	8.20	8.54	8.98	9.30	9.70	10.10	10.40	10.75	11.10	11.45
ϵ'' (9.62 GHz)	0.63	0.75	0.89	1.03	1.23	1.43	1.67	1.95	2.24	2.60
ϵ' (26.62 GHz)	7.80	8.06	8.29	8.50	8.67	8.73	8.70	8.59	8.47	8.35
ϵ'' (26.62 GHz)	1.75	1.97	2.24	2.55	2.87	3.23	3.60	3.96	4.33	4.75
CP	0.402	0.434	0.462	0.507	0.566	0.627	0.703	0.803	0.932	1.089

Far-infrared measurements are available from Chemistry Department, University of Wales, Aberystwyth at the same state points.

REFERENCES

Bellemans, A., Ciccotti, G., and Ryckaert, J. P., *Mol. Phys.* **44**, 979 (1981).

Berendsen, H. J. C., van Gunsteren, W. F., and Rullmann, J. A. C., *Mol. Phys.* **44**, 69 (1981).

Böttcher, C. J. F. and Bordewijk, P., *Theory of Electric Polarisation*, Elsevier, Amsterdam (1979).

Bridgman, P. W., *J. Chem. Phys.* **9**, 794 (1940).

Brier, P. N. and Perry, A., *Adv. Mol. Rel. Int. Proc.* **13**, 1 (1977).

Caloin, M. and Candam, S., *J. Phys.* (*Paris*) **33**, 7 (1972).

Chantry, G. W., *Submillimetre Spectroscopy*, Academic Press, London (1971).

Coffey, W. T., Rybarsch, C., and Schröer, W., *Phys. Letts.* **88A**, 331 (1982).

Coffey, W. T., and Calderwood, J. H., *Proc. R. Soc. Lond.*, **356A**, 269 (1977).

Debye, P., *Polar Molecules*, Chem. Cat. Co., New York (1929).

Evans, M. W., *Chem. Phys. Lett.* **39**, 601 (1976).

Evans, M. W., *J. Chem. Phys.* **76**, 5473 (1982).

Evans, M. W., *J. Chem. Phys.* **76**, 5480 (1982).

Evans, M. W., *J. Chem. Phys.* **77**, 4632 (1982), **78**, 925, **78**, 5403 (1983).

Evans, M. W. and Yarwood, J., *Adv. Mol. Rel. Int. Proc.* **21**, 1 (1981).

Evans, M. W., Evans, G. J., Coffey, W. T., and Grigolini, P., *Molecular Dynamics*, Wiley-Interscience, New York (1982).

Haken, H., *Synergetics*, Springer-Verlag, Berlin (1977).

Hildebrand, J., Faraday Symp., Univ. of Kent., 1978.

Kell, D., Dept. of Molecular Biology, U.C.W., Aberystwyth, personal communication (1981).

Kramers, H. A., *Physica* **7**, 284 (1940).

Kubo, R., *Rep. Prog. Phys.* **29**, 255 (1966).

Laubereau, A., Fischer, S. F., Spanner, K., and Kaiser, W., *Chem. Phys.* **31**, 335 (1978).

Mori, H., *Prog. Theor. Phys.* **33**, 423 (1965); **34**, 399 (1965).

Mori, H., Fujisaka, H., and Shigematsu, H., *Prog. Theor. Phys.*, **51**, 109 (1974).

Mori, H., Nagano, K., Karasudani, T., and Okamoto, H., *Prog. Theor. Phys.* **63**, 1904 (1980).

Muller, H. D. and Rothschild, W., *Far Infrared Spectroscopy*, Wiley-Interscience, New York (1971).

Reid, C. J. and Evans, M. W., *J. Chem. Soc., Faraday Trans. II* **75**, 1213 (1979).

Reid, C. J. and Evans, M. W., *Mol. Phys.* **40**, 1357 (1980).

Risken, H. and Vollmer, H. D., *Z. Phys. B* **31**, 209 (1978).

Sandhu, H. S., *J. Magn. Res.* **29**, 563 (1978).

Sutter, H., *Dielectric and Related Molecular Processes*, Chem. Soc., London, Vol. 1 (1972).

van der Avoird, A., Mulder, F., Wormer, P. E., and Berns, R. M., "Ab Initio Studies of the Interactions in van der Waals Molecules", *Topics in Current Chemistry*, M. J. S. Dewar et al., Eds., Springer-Verlag, Berlin (1980).

van Kampen, N. G., *Phys. Rep.* **24C**, 171 (1976).

van Konynenburg, P., and Steele, W. A., *J. Chem. Phys.* **56**, 4775 (1972).

van Woerkom, P. C. M., de Bleyser, J., de Zwart, M., Burgess, P. M. J., and Leyte, J. C., *Ber. Bunsenges. Phys. Chem.* **78**, 1303 (1974).

Zwanzig, R. and Nordholm, S., *J. Stat. Phys.* **13**, 347 (1975).

CHAPTER TWO

Computer Simulation of Liquid CH_2Cl_2

2.1. INTRODUCTION

The fundamental idea of computer simulation is to take a *limited* number of molecules and then to *solve numerically* the equations governing their motion. The number of molecules used in the simulation is in the region of 100 to 1000. Thus a considerable amount of computer speed and power is needed in order to construct the trajectory of each molecule of the sample. It is assumed that the dynamics of an individual molecule may be adequately described by the equations of classical mechanics, namely Hamilton's equations (Goldstein, 1950). The Hamiltonian is constructed as the sum of the kinetic and potential energies in the usual way. It is, however, very difficult to obtain an exact form for the potential energy. Thus it is invariably supposed that the potential energy in the Hamiltonian may be constructed using the assumption of *pairwise additivity*. This means that the technique cannot yet cope satisfactorily with the effects of polarizability (Evans et al., 1982). This is *not* a pairwise additive phenomenon on a molecular level. Finney (1978) and his group have taken the first steps toward removing this constraint in their machine simulations of water.

The trajectory of one particular CH_2Cl_2 molecule is determined via the equation of motion, by all the other molecules in the liquid sample. If our simulation algorithm is for 108 molecules (a commonly used number), the trajectory of one of them is ideally determined by calculating its interaction with the other 107. The most important part of this interaction, however, is that arising from the interaction of the molecule with its nearest-neighbor shell (usually consisting of about eight or so others). The more distant molecules have progressively less influence. It is therefore assumed that the long-range part of the potential energy generated by the electron cloud of a molecule may be set to equal zero at a certain cutoff distance R. The more dipolar a molecule, the less satisfactory, in general, are the assumptions both of pairwise additivity (due to polarizability affects) and of cutoff of the molecule's potential energy (*Molecular Dynamics*, Chapters 3 and 4). An intensive programming effort is currently being directed toward developing a computer simulation algorithm in order to try to compensate some of the newer algorithms for these approximations. For example, those of the Science and

Engineering Research Council's CCP5 Group use Ewald summations in order to deal with long-range effects such as the charge–charge interaction.

The other common approximation in the computer-simulation method is the use of *periodic boundary conditions*. These arise out of the need for maintaining our 108 molecules within the confines in which they were held captive at the start of the simulation. The container in which the molecules are located may be a cube out of the sides of which the molecules would rapidly escape if allowed to. The periodic boundary conditions are Boolean statements written into the simulation algorithm. They ensure that, as one molecule leaves the cube, another enters at the opposite side in order *to keep the total energy constant*.

We do not propose to go deeply into the technical details of the algorithm TETRAH used for liquid CH_2Cl_2 in this chapter. However, one of the most important criteria used for assessing the efficacy of a molecular-dynamics algorithm is whether or not the total energy is constant. The root-mean-square deviation from the mean value of this quantity should be well below the thermal energy kT at a given temperature T. The temperature in a molecular-dynamics simulation is calculated from the equipartition theorem—that is, from the total kinetic energy arising from *all* sources (namely the rotational and translational motion). In order to drive TETRAH to the required temperature the method of *temperature scaling* is used. This is equivalent to applying a thermostat to the 108 molecules. The kinetic energy for a fixed sample volume is adjusted until equilibrium is attained near the required temperature. The total energy and pressure [calculated from the relevant macroscopic equations (Cheung, (1978)] should reach equilibrium without further rescaling. Once the sample has attained equilibrium, we can begin the process of extracting spectral information from a given model of the potential-energy profile of the molecule. The power of the rescaling method is such that every conceivable spectrum can be computed (from the 108 trajectories stored on tape) in a self-consistent manner from the *same* intermolecular potential. Some of these spectra are observable experimentally, but others are not (or only very indirectly). Computer simulation can therefore provide us with insights into aspects of molecular dynamics (used in the traditional sense of the term) which may hitherto have eluded both experimentalist and theoretician. An example is the behavior of translational–rotational autocorrelation functions (a.c.f.'s) in a moving frame of reference. (Bellemans et al., 1982).

2.2. CORRELATION FUNCTIONS FROM TETRAH

Another advantage of the computer method is the facility it provides for the calculation of correlation functions without the need for linear-response theory or the fluctuation–dissipation theorem. The analytical results gained from models of the liquid state can therefore be tested directly. This is important when we come to deal with nonlinear phenomena as discussed at the end of Chapter 1.

For spectra of interest to us, such as those of the far infrared, the fluctuation–dissipation theorem provides a direct link with the relevant correlation function of molecular motion (Evans et al., 1982). The problems of data interpretation can revolve around the nature of the correlation function. For example, can the correlation function of interest be adequately approximated by the autocorrelation function? This question cannot be answered in full, but the computer simulation does provide *well-defined* auto- and cross-correlation functions. These can be compared with both the spectral data and the available theory.

The correlation function is calculated in a computer simulation using a running time average (Evans et al., 1982). For a statistically stationary process, this quantity is equal to the ensemble average. The process is illustrated in Fig. 2.2.1. The equations of motion are integrated using finite time steps in digital computers. One picosecond in the real lifetime of a particular correlation function is made up of hundreds of time steps. Every few time steps the dynamical information is stored on magnetic tape for further analysis.

Here we describe the simulation of the molecular dynamics of CH_2Cl_2 in the liquid state using a model representation of the intermolecular potential. This consists of a 5×5 atom–atom Lennard-Jones potential with or without fractional charges at the atomic sites. Thermodynamic and spectroscopic data indicate that this potential is most acceptable. The effect of adding charges is significant but not pronounced. For example, the simulated far-infrared spectrum appears more realistic after an attempt has been made to include charge–charge interactions. More accurate representation of the intermolecular pair potential of CH_2Cl_2 is needed in order to match the far-infrared results. Improvement might be obtained by measuring the second dielectric virial coefficient of CH_2Cl_2 over a sufficient temperature range (Sutter, 1972).

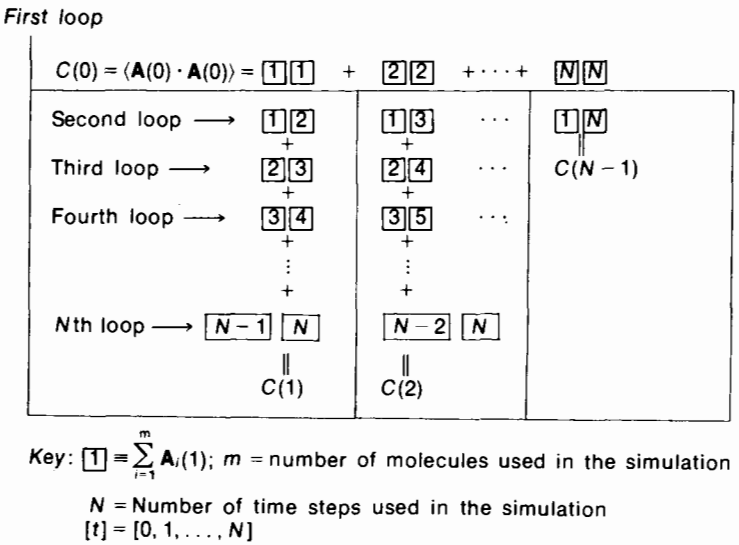

FIGURE 2.2.1. Construction by computer of a correlation function of the dynamical variable $\mathbf{A}(t)$.

Our knowledge of the potential-energy surface between interacting molecules of the size of CH_2Cl_2 is poor despite extensive research on the subject. The difficulty of finding the shape of the surface is due to a number of factors. The greatest task is that of relating the pair potential to measurable data in a mathematically and physically rigorous manner. Thus, in the absence of a quantitative expression for the potential energy of two interacting CH_2Cl_2 molecules, computer simulation relies on semiempirical forms for that quantity. A popular method is to represent the interaction between each pair of atoms from two different molecules by a Lennard-Jones potential. The complete pair potential is a sum of atom–atom terms. This is supposed to cover both the dispersive and the repulsive part of the potential (van der Avoird et al., 1980). The electric parts of the potential are represented by fractional charges at each atomic site. This is much easier than expanding the electric potential in multipole moments (Kielich, 1972), especially for asymmetric tops such as CH_2Cl_2. The drawback associated with using charges springs from the technical difficulty of dealing with long-range interaction in a molecular-dynamics simulation using periodic boundary conditions.

2.2.1. Detailed Description of the Algorithm

The equations of motion of 108 molecules are solved using a third-order Newton expansion and a simple quadrature routine based on the Verlet algorithm. The time step is usually of the order of 5×10^{-15} s (0.005 ps). The information on tape is then used to construct time autocorrelation functions of various kinds with the usual running time averages. Autocorrelation functions, which are often constructed, are those of $\vec{v}$ the center-of-mass linear velocity; those of the unit vectors $\vec{e}_A, \vec{e}_B, \vec{e}_C$ along the principal axes of inertia; and those of their derivatives $\dot{\vec{e}}_A, \dot{\vec{e}}_B, \dot{\vec{e}}_C$. These latter a.c.f.'s may be computed using the fact that the time rate of change of the unit vector $\vec{e}_{A,B,C}$ fixed in the molecule is given by the kinematic relation

$$\dot{\vec{e}}_{A,B,C} = \vec{\omega} \times \vec{e}_{A,B,C} \tag{2.2.1.1}$$

Here $\vec{\omega}$ is the angular velocity of the molecule. The vector a.c.f. $\langle \vec{e}_A(t) \cdot \vec{e}_A(0) \rangle$ (if a dipole lies along that vector) is related by direct Fourier transformation to the far-infrared power absorption coefficient $\mathfrak{A}(\bar{\nu})$ in neper cm^{-1}. The spectrum $\mathfrak{A}(\bar{\nu})$ is an accurate test of the theory of rotational diffusion in molecular liquids. The autocorrelations $\langle \vec{e}_A(t) \cdot \vec{e}_A(0) \rangle$, $\langle \vec{e}_B(t) \cdot \vec{e}_B(0) \rangle$, and $\langle \vec{e}_C(t) \cdot \vec{e}_C(0) \rangle$ are obtained by simulation. These have areas τ_1, τ_2, and τ_3 respectively. The friction coefficients β_1, β_2, and β_3 of the theory of Brownian motion may be estimated using the relations between relaxation times and the diffusion coefficients (Evans et al., 1982), namely,

$$\begin{aligned} \tau_1^{-1} &= D_2 + D_3 \\ \tau_2^{-1} &= D_1 + D_3 \\ \tau_3^{-1} &= D_1 + D_2 \end{aligned} \tag{2.2.1.2}$$

where $D_i = kT/I_i\beta_i$. Knowing β_1, β_2, and β_3, we can then aim to reproduce a range of computer simulation curves theoretically. This is done without recourse to a fitting procedure and with no free parameters.

The algorithm TETRAH was originally written by Singer et al. Ferrario (1981) has modified this algorithm to include a charge–charge interaction. This also includes a force cutoff criterion based on molecular center-of-mass-to-center-of-mass cutoff. For CH_2Cl_2 at 293 K and 1 bar, for example, this cutoff radius is 11.28 Å. The equations of motion in the modified TETRAH are solved with a third-order predictor algorithm. This coincides with the two-step Verlet algorithm as far as the translational motion of the center of mass is concerned. The rotation is determined using as coordinates the angular momentum and the three unit vectors along the principal axes. The Lennard-Jones parameters (Hirschfelder, Curtiss, and Bird, 1964) are

$$\sigma(\text{H–H}) = 2.75 \text{ Å}, \qquad \sigma(\text{Cl–Cl}) = 3.35 \text{ Å}$$

$$\sigma(\text{C–C}) = 3.20 \text{ Å}, \qquad \frac{\epsilon}{k}(\text{H–H}) = 13.4 \text{ K}$$

$$\frac{\epsilon}{k}(\text{Cl–Cl}) = 175.0 \text{ K}, \qquad \frac{\epsilon}{k}(\text{C–C}) = 51.0 \text{ K}$$

The fractional charges (when incorporated) are

$$+0.098|e| \text{ on H}, \qquad -0.109|e| \text{ on Cl}, \qquad +0.022|e| \text{ on C}$$

$$e = -1.6 \times 10^{-19} \text{ C}$$

$|e|$ is the absolute value of the charge on the electron.

The former values were chosen in order to optimize the thermodynamic results from TETRAH. The latter were obtained from a simple molecular-orbital calculation by del Re (1958). The molecules were initially set up on a face-centered lattice. This was allowed to melt over approximately 2000 time steps of 0.005 ps each. The main runs were carried out in sections of roughly 10 minutes CPU time on Manchester University's (U.M.R.C.C.) CDC 7600 computer with up to 10,000 time steps.

Instantaneous values of thermodynamic quantities are recorded in TETRAH. Average values over the complete equilibrium run are also computed. The total pressure and specific heat at constant volume (for example) are calculated using the expressions given by Cheung (1978). Some typical output parameters for a programmed molar volume corresponding to 293 K and 1 bar are as follows:

1. The averages (omitting charges) computed over 3600 time steps are the temperature (T), pressure (P), internal energy (U), total energy (E_T), and specific heat at constant volume (C_v). We have $\langle T \rangle = 292.7 \pm 9.2$ K (49.5%

translational and 50.5% rotational); $\langle P \rangle = 283 \pm 312$ bar; $\langle U \rangle = -23.69$ kJ mole^{-1}; $\langle E_T \rangle = -(16.39 \pm 0.21)$ kJ mole^{-1}; $\langle C_v \rangle = 37$ J mole^{-1} K^{-1}.

2. Having repeated the simulation (this time including charges), we find $\langle T \rangle = 294.5 \pm 11.0$ K (50.2% translational, 49.8% rotational); $\langle P \rangle = 273 \pm 300$ bar; $\langle U \rangle = -25.46$ kJ mole^{-1}; $\langle E_T \rangle = -(18.11 \pm 0.13)$ kJ mole^{-1}; $\langle C_v \rangle = 46.0$ J mole^{-1} K^{-1}.

Therefore *both* the total energy and the potential energy are *significantly* affected by the inclusion of charges in the algorithm. So also are the atom–atom pair distribution functions (Section 2.2.2). C_v is a fluctuating quantity (i.e. $\Delta U/\Delta T$). Ideally it needs runs of at least 20,000 time steps for a good statistical sample of its behavior. The inclusion of charges brings the computed values closer to that determined by experiment, namely 90 J mole^{-1} K^{-1}.

2.2.2. Atom – Atom Pair Distribution Functions

These distribution functions are available, both with and without charges, from the TETRAH algorithm. They essentially measure the probability of finding another atom (A) at a distance r from a given atom (B) on another molecule at thermodynamic equilibrium. If the probability distribution function (p.d.f.) has a two- or three-peak structure, then this implies that the liquid CH_2Cl_2 has substantial residual (short range only) ordering compared with the crystalline lattice; see Fig. 2.2.2.1. This result is for the p.d.f. describing H–H atom–atom positions. It is not certain if this structure may be attributed solely to the repulsive parts of the intermolecular potential. This is because the addition of charges inhibits the first peak (2.8 Å). At the same time it enhances the second

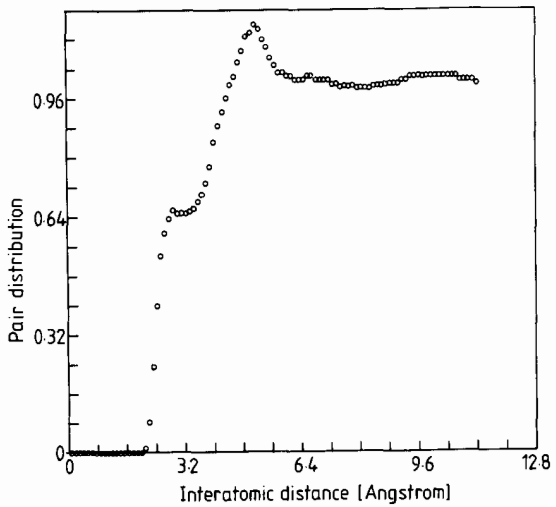

FIGURE 2.2.2.1. Hydrogen-to-hydrogen atom–atom pair distribution function extracted as a mean over the equilibrium 5 × 5 potential: no charges, 293 K, 1 bar.

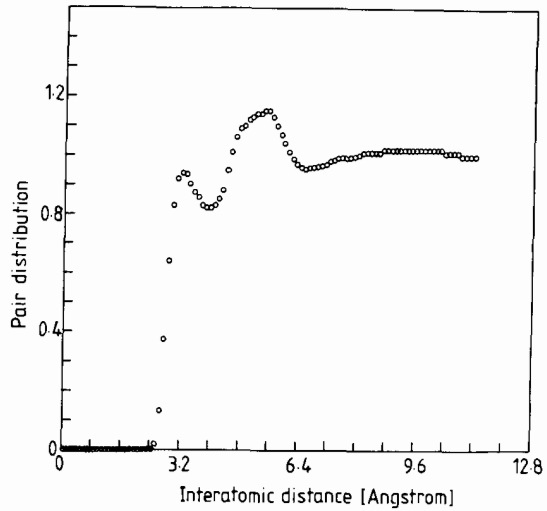

FIGURE 2.2.2.2. As in Fig. 2.2.2.1: hydrogen to chlorine.

peak. Measurements (during the course of the Delta project) on isotropically substituted CH_2Cl_2 should provide an experimental test of the simulation. They should also improve our knowledge of the intermolecular potential itself. Similarly Figs. 2.2.2.2 to 2.2.2.6 reflect the sensitivity of the structure of the p.d.f. to the electric parts of the pair potential. Thus the first peak in the H–Cl p.d.f. is increased while that for H–C is decreased. Likewise the second peak in Cl–Cl is sharpened and the shoulder in Cl–C is decreased. The main peak in C–C is only slightly sharpened.

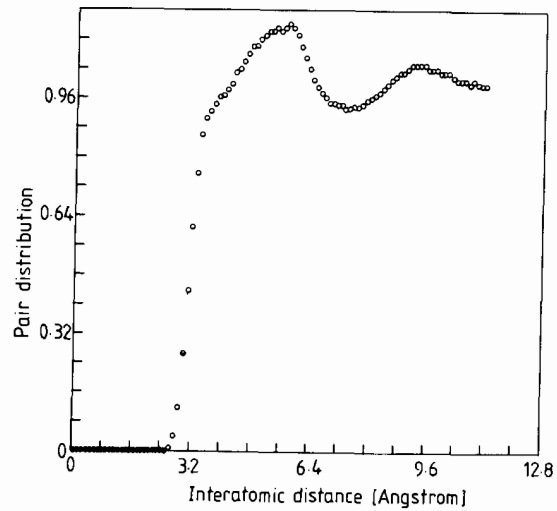

FIGURE 2.2.2.3. As in Fig. 2.2.2.1: hydrogen to carbon.

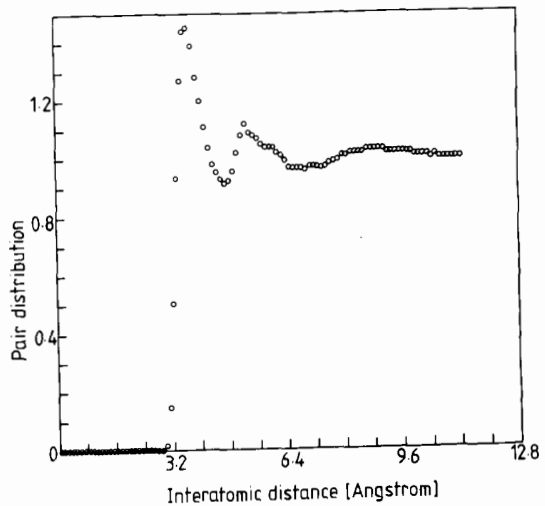

FIGURE 2.2.2.4. As in Fig. 2.2.2.1: chlorine to chlorine.

2.2.3. Dynamical Results

A discriminating test for computer simulation is provided by comparing the simulated far-infrared power absorption coefficient with observations of that quantity. Figure 2.2.3.1 shows such a comparison. The simulated spectrum is somewhat affected by artifacts introduced as a result of the numerical Fourier transformation of $\langle \dot{\vec{e}}_A(t) \cdot \dot{\vec{e}}_A(0) \rangle$. It is clear that the 5×5 algorithm is a more realistic representation of the observed data than the Debye theory of rotational diffusion (*Molecular Dynamics*, Chapter 2). This theory was not de-

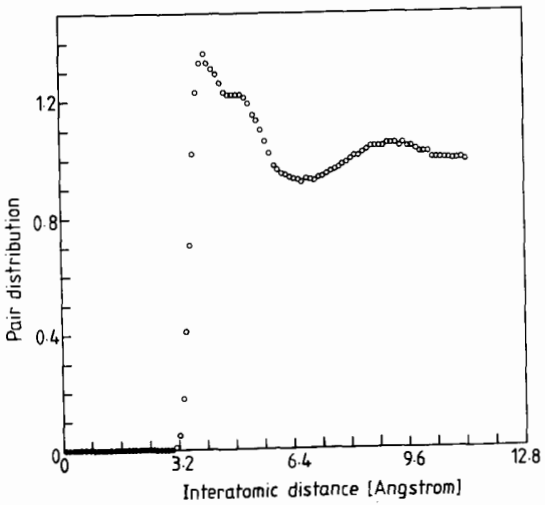

FIGURE 2.2.2.5. As in Fig. 2.2.2.1: chlorine to carbon.

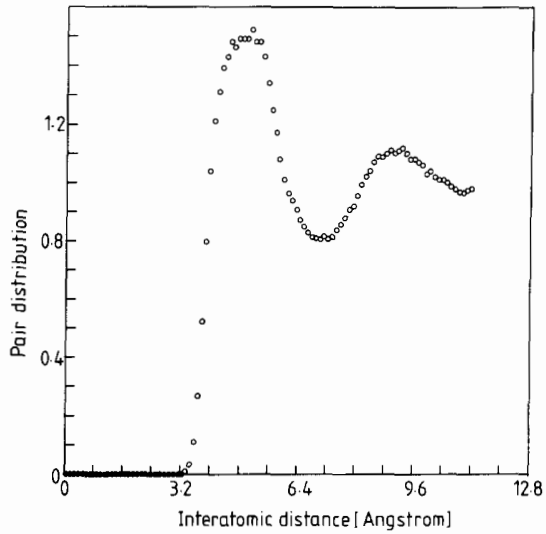

FIGURE 2.2.2.6. As in Fig. 2.2.2.1: carbon to carbon.

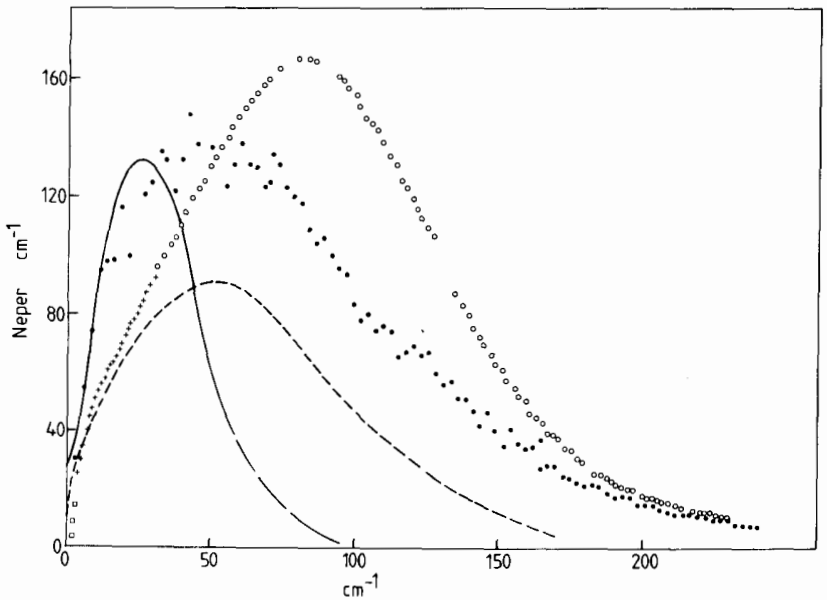

FIGURE 2.2.3.1. Comparison of molecular-dynamics simulation and far-infrared spectra of CH_2Cl_2, pure and in solution in CCl_4. O and +: measured data (interferometers and klystrons); ●: computer simulation, 5×5 potential, no charges; solid + long-dashed curve: computer simulation, 3×3 potential, no charges; short-dashed curve: exptl. data, 10% solution in CCl_4.

signed to cope with such high-frequency regions. The simulated curve (●) in Fig. 2.2.3.1 has been derived from an autocorrelation function. In addition the intensity of the simulated spectrum was estimated using the observed static dielectric permittivity for pure CH_2Cl_2, $\epsilon_s = 9.02$ (*Molecular Dynamics*, Chapter 4), with Scaife's internal-field correction (Scaife, 1964, 1971). We obtain the spectrum from the cross-correlation function by Fourier transformation of $\langle \dot{\vec{e}}_A(0) \cdot \sum_{i=1}^{n} \dot{\vec{e}}_{A_i}(t) \rangle$. On computation of this within a sphere of 8-Å radius, the spectrum changes slightly in position.

In Fig. 2.2.3.2 we have plotted the numerical Fourier transform of $\langle \dot{\vec{e}}_A(t) \cdot \dot{\vec{e}}_A(0) \rangle$ from the 5×5 algorithm without charge interactions directly onto the spectrum of 10% CH_2Cl_2 in dilute decalin taken by Reid and Evans (1980). The two curves have been normalized for clarity. It appears that this match is excellent except in the high-frequency wing. There, the simulated spectrum decays more slowly. The microwave correlation time (the inverse of the dielectric-loss peak frequency) measured by Reid for CH_2Cl_2 in 10% decalin solution is 1.2 ± 0.3 ps. The area under the simulated correlation function $\langle \vec{e}_A(t) \cdot \vec{e}_A(0) \rangle$ is also 1.2 ps. From these results we may reason as follows:

1. The hydrogen atoms appear to govern the dynamics of CH_2Cl_2.
2. Figure 2.2.3.2 is a comparison of a computer simulation of neat CH_2Cl_2 liquid omitting the electric (charge–charge) interaction with an experimentally observed spectrum of CH_2Cl_2 in dilute decalin solution. Here the electrical interactions appear, therefore, to have been effectively isolated from the kinematics. In other words in a dilute CH_2Cl_2–decalin solution, we may suppose that we are observing the *autocorrelation function* of CH_2Cl_2 with *negligible* multipole–multipole interaction or cross correlation between CH_2Cl_2 molecules.
3. The similarity of the bandshapes in Fig. 2.2.3.2 suggests that induced-absorption effects play a minimal part in the behavior of the spectrum of CH_2Cl_2 in dilute decalin solution. In order to corroborate these results we need more accurate experimental spectra than those obtained by Reid and Evans (1980).

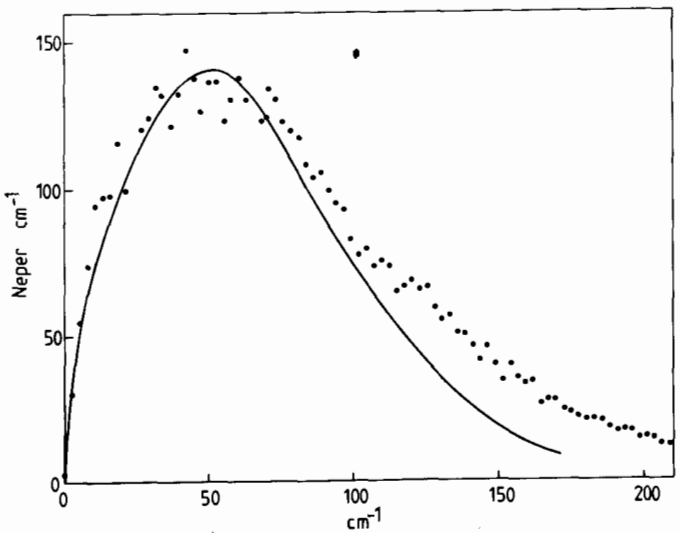

FIGURE 2.2.3.2. Comparison of simulation (●) and scaled-up spectrum (solid curve) of CH_2Cl_2

The orientational autocorrelation functions P_1 and P_2 (Legendre polynomials) are illustrated in Fig. 2.2.3.3(a) and (b). These are for the vectors $\vec{e}_A$, $\vec{e}_B$, and $\vec{e}_C$ fixed in the principal moment-of-inertia frame of the CH_2Cl_2 molecule. The decay with time of the a.c.f.'s of $\vec{e}_A$ and $\vec{e}_C$ is similar. That of $\vec{e}_B$ is much slower. The areas under the curves in Fig. 2.2.3.3(b) may be related in a straightforward manner to NMR correlation times in CH_2Cl_2 (Brier and Perry, 1977). This may be done using the nuclear magnetic resonances of C, Cl, H, and D. However, we have mentioned in Chapter 1 that the available experimental data are not in accord from one group to another. Ideally, then, the correlation times for all the available isotopes should be remeasured over a wide range of temperatures *and* hydrostatic pressures.

In Fig. 2.2.3.4(a) we plot the first four autocorrelation functions of orientation from two representations of the CH_2Cl_2 potential energy. These are the 5×5 atom–atom potential described already, and also a 3×3 atom–atom

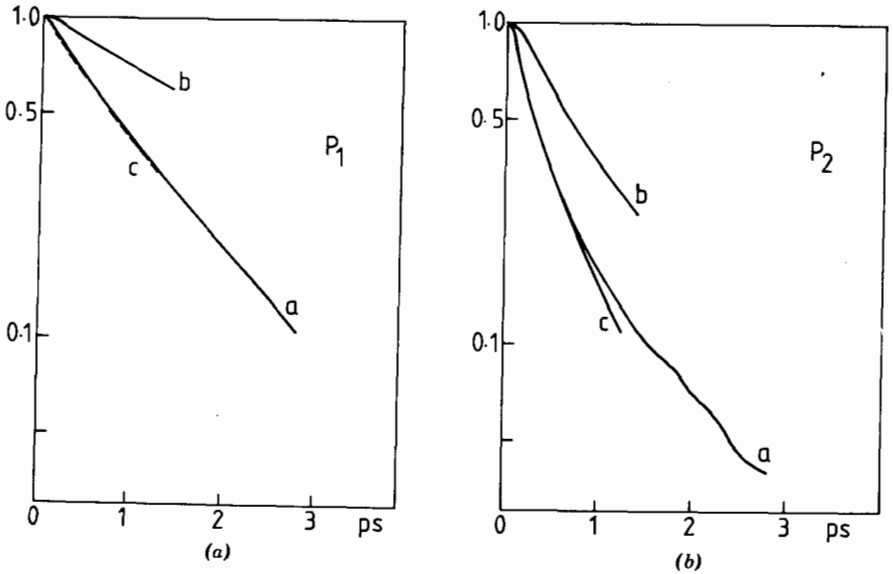

FIGURE 2.2.3.3. (a) 5×5 potential, no charges. Orientational a.c.f. P_1 of: the dipole unit vector $\vec{e}_A$ (curve *a*) the orthogonal vector $\vec{e}_B$ (curve *b*); the mutually orthogonal vector $\vec{e}_C$ (curve c). (b) NMR a.c.f.'s P_2; curve labels as in (a).

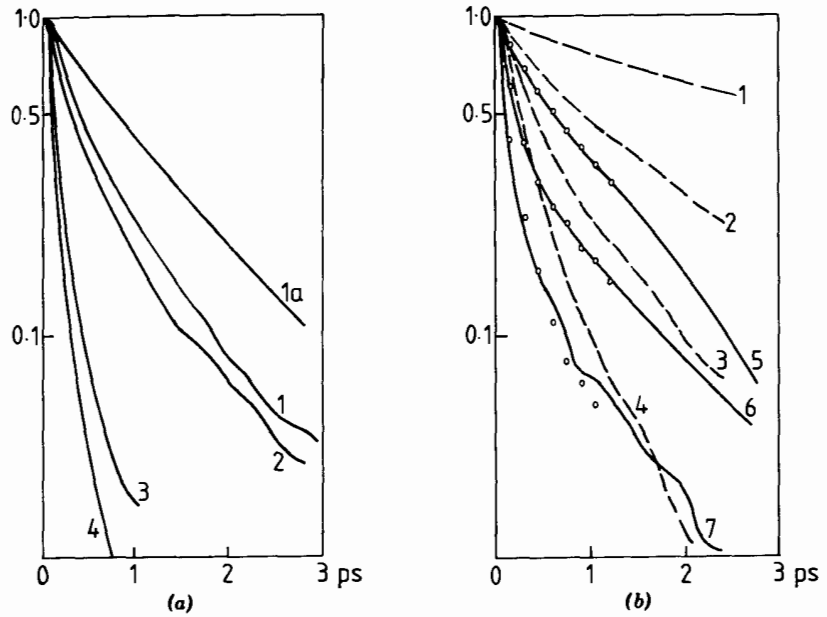

FIGURE 2.2.3.4. (a) Curves 1 to 4: a.c.f.'s P_1 to P_4 of $\vec{e}_A$, 3 × 3 potential, no charges. For comparison, curve 1a is the P_1 a.c.f. of $\vec{e}_A$ from the 5 × 5 potential, no charges. (b) 3 × 3 potential, no charges, at 5 kbar, 323 K. Curves 1 to 4: a.c.f.'s P_1 to P_4 of $\vec{e}_B$. Curves 5 to 7: a.c.f.'s P_1 to P_3 of $\vec{e}_A$ (solid curves) and of $\vec{e}_C$ (○).

potential where CH_2 is regarded as a single entity. It is evident that the 3 × 3 algorithm produces nonexponential a.c.f.'s which decay too rapidly even when compared with the experimental data on CH_2Cl_2 in dilute decalin solution. It is interesting despite this discrepancy to inquire into the difference between Fig. 2.2.3.4(a) and (b). In the latter we show the results of simulating P_1 to P_4 for $\vec{e}_A$, $\vec{e}_B$, and $\vec{e}_C$ from the 3 × 3 algorithm at 5000 bar and 323 K, relative to those in Figure (a). The a.c.f.'s in (b) decay more slowly. The anisotropy between $\vec{e}_B$ and $\vec{e}_A$ or $\vec{e}_C$ has increased. This indicates what should be experimentally observable when techniques become available for the measurement of P_1 to P_4 under hydrostatic pressure.

Figure 2.2.3.5 illustrates the a.c.f. $\langle \dot{\vec{e}}_A(t) \cdot \dot{\vec{e}}_A(0) \rangle$ calculated from both the 3 × 3 and 5 × 5 algorithms. In this figure these a.c.f.'s are compared with the Fourier transform of the far-infrared power absorption coefficient for a 10% v/v solution of CH_2Cl_2 in decalin. The experimental curve is deeper and slightly more oscillatory than the simulated ones. In Fig. 2.2.3.6 we illustrate the angular-momentum autocorrelation function $\langle \vec{J}(0) \cdot \vec{J}(t) \rangle / \langle J^2(0) \rangle$ from the 3 × 3 algorithm compared with $\langle \dot{\vec{e}}_A(t) \cdot \dot{\vec{e}}_A(0) \rangle$ computed under the same conditions (293 K, 1 bar). These are also compared with the inverse Fourier transform of the far infrared absorption coefficient $\mathfrak{A}(\bar{\nu})$ in neat and dilute solution. The angular-momentum a.c.f. has a weak but long positive tail. The

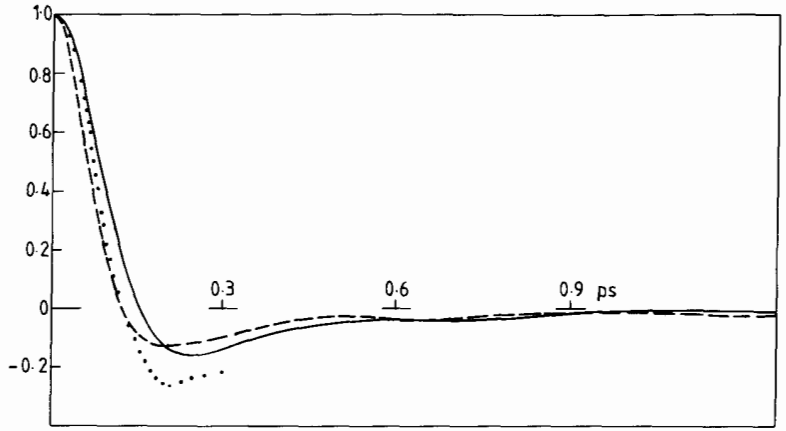

FIGURE 2.2.3.5. Rotational velocity a.c.f.'s of $\dot{\vec{e}}_A(t)$. Solid curve: 3 × 3 potential, no charges; dashed curve: 5 × 5 potential, no charges; dotted curve: 10% v/v CH_2Cl_2 in CCl_4.

rotational-velocity a.c.f. has a corresponding long *negative* tail. Long tails make it difficult to calculate inverse Fourier transforms numerically without introducing artifacts. There is a difference between the decay times of each function. This difference has decreased (Fig. 2.2.3.7) at 5000 bar, 323 K. In Fig. 2.2.3.7, the functions show a more pronounced oscillation. Further, the simulated far-infrared spectrum shifts to a higher frequency.

It is interesting from a theoretical point of view to use the 5 × 5 algorithm to extract, at 293 K and 1 bar, angular-velocity and angular-momentum a.c.f.'s

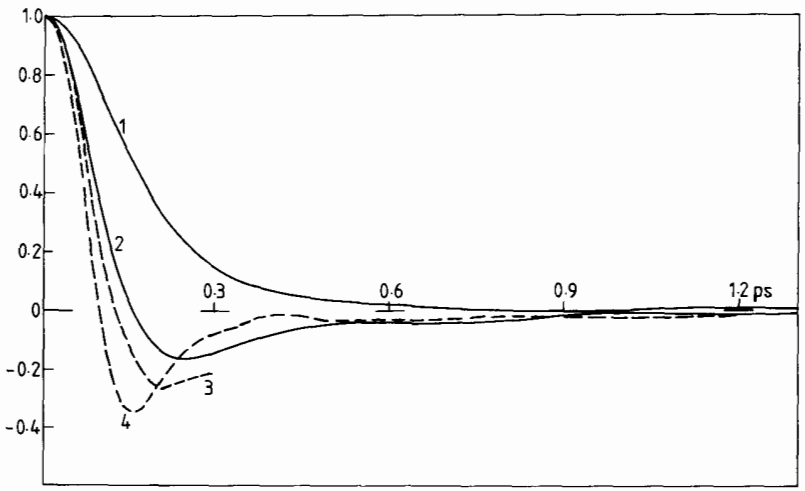

FIGURE 2.2.3.6. Comparison of angular-momentum a.c.f. (curve 1) with the a.c.f. of $\dot{\vec{e}}_A(t)$ (curve 2) and with the rotational-velocity a.c.f.'s from CH_2Cl_2 data in solution and in pure liquid state (curves 3 and 4 respectively). Normalized as usual to 1 at $t = 0$. 3 × 3 potential, no charges.

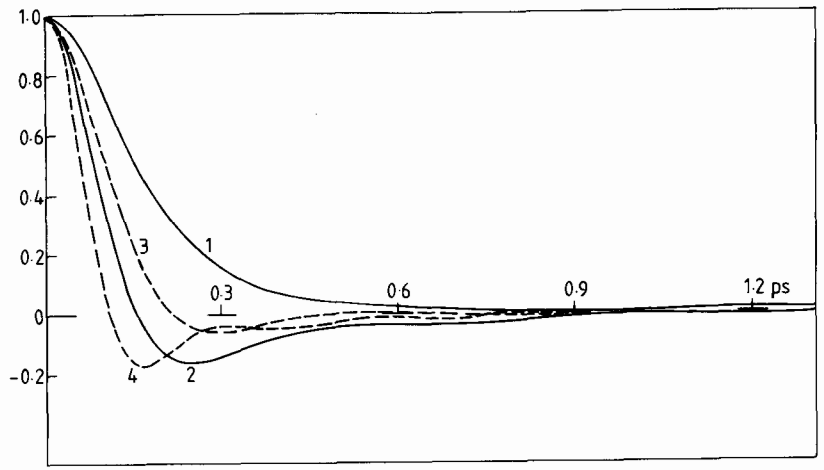

FIGURE 2.2.3.7. Angular-momentum and $\vec{e}_A(t)$ a.c.f.'s respectively at 1 bar 293 K (curves 1 and 2); at 5 kbar, 323 K (curves 3 and 4). 3 × 3 potential, no charges.

in both the laboratory and molecular frames. These are fixed by the moment-of-inertia principal axes, labeled 1, 2, and 3 for $\vec{e}_A$, $\vec{e}_B$, and $\vec{e}_C$ respectively. The angular momentum a.c.f.'s in this molecule-fixed frame are illustrated in Figs. 2.2.3.8–2.2.3.10. The a.c.f.'s of the mean squared values are also illustrated. The correlation times about the second principal axis are the shortest. This corresponds to the smallest principal moment of inertia. We note that when $t \to \infty$ the limit of the mean values of the a.c.f.'s, when squared, is about $\frac{1}{3}$. This corresponds (Berne and Harp, 1970) to *equilibrium* statistics, which are

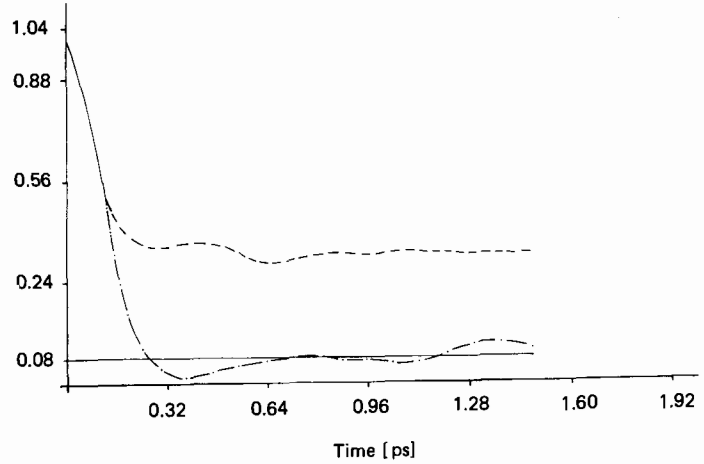

FIGURE 2.2.3.8. 5 × 5 algorithm, no charges. Angular-momentum a.c.f. in the molecule frame. Lower curve: component in the axis direction of $\vec{e}_C$, i.e. $\langle J_1(t)J_1(0)\rangle$, normalized at $t = 0.293$ K, 1 bar. Upper curve: $\langle J_1^2(t)J_1^2(0)\rangle/\langle J_1^4\rangle$.

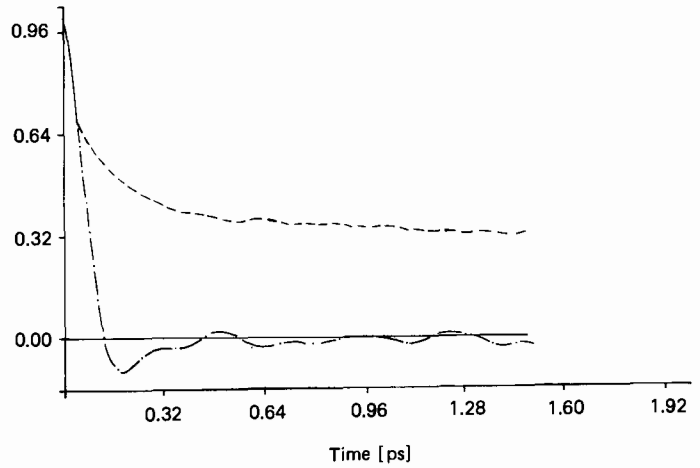

FIGURE 2.2.3.9. As in Fig. 2.2.3.8, but a.c.f. component along the $\vec{e}_B$ axis. Note the faster decay.

Gaussian. The transient behavior of this a.c.f. is *not* Gaussian, however. The a.c.f. of the angular momentum in the laboratory frame is illustrated in Fig. 2.2.3.11. The angular-velocity a.c.f.'s are illustrated, for comparison, in Fig. 2.2.3.12. The torque and its squared-value a.c.f.'s show more pronounced oscillations than the others (Fig. 2.2.3.13).

The orientational autocorrelation functions obtained from the 5 × 5 molecular-dynamics simulation TETRAH are described by Figs. 2.2.3.14–2.2.3.16. Figures 2.2.3.14 and 2.2.3.16 illustrate P_1 and P_2 for the dipole vector and the vector for the axis which has the greatest principal moment of inertia. The correlation time of the latter a.c.f. (Fig. 2.2.3.15) is much the longer, just as in

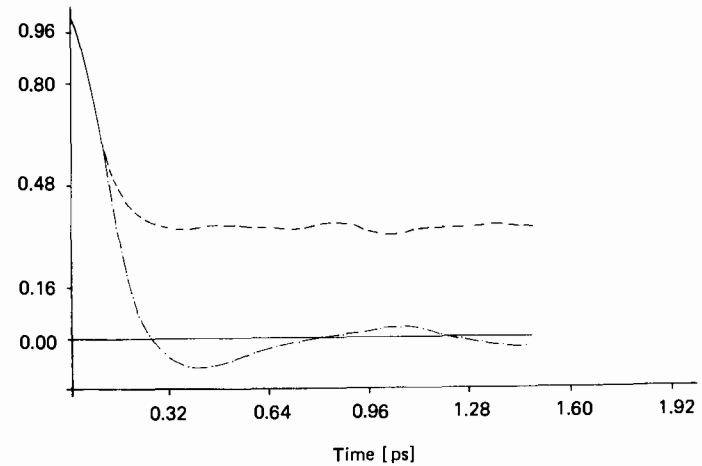

FIGURE 2.2.3.10. As in fig. 2.2.3.8, but along $\vec{e}_A$.

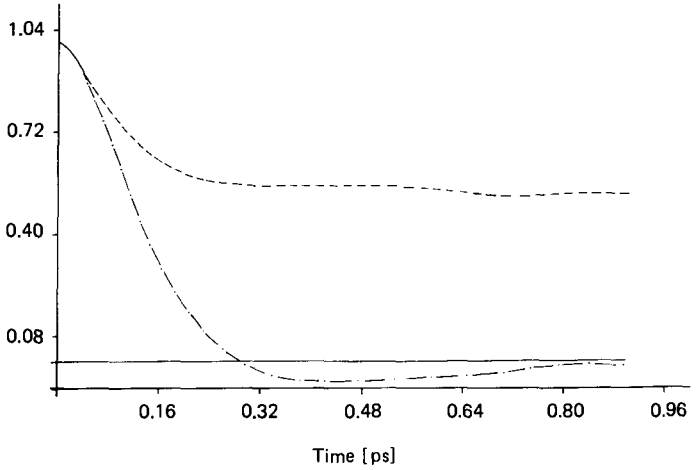

FIGURE 2.2.3.11. Lower curve: total-angular-momentum a.c.f. [of $J(t)$], laboratory frame, 5 × 5 potential, no charges, 293 K, 1 bar. Upper curve: a.c.f. $\langle J^2(t)J^2(0)\rangle/\langle J^4(0)\rangle$, 5 × 5 potential, no charges.

the 3 × 3 case. The theoretical model reproduces the simulation data very closely. Figure 2.2.3.17 illustrates the rotational-velocity a.c.f. for the vector $\vec{e}_A$,

$$\{\langle \dot{\vec{e}}_A(t)\cdot\dot{\vec{e}}_A(0)\rangle/\langle \dot{\vec{e}}_A(0)\cdot\dot{\vec{e}}_A(0)\rangle\},$$

parallel to the dipole vector. This is oscillatory with a long negative tail.

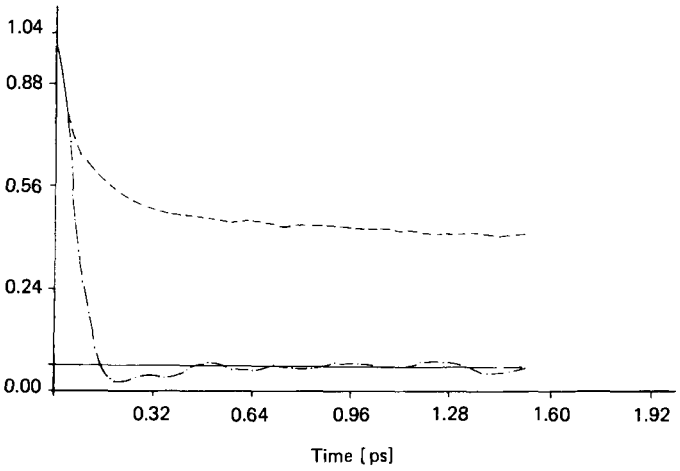

FIGURE 2.2.3.12. Lower curve: Angular-velocity a.c.f. [of $\vec{\omega}(t)$], laboratory frame. Slightly different than that of $\vec{J}(t)$. 5 × 5 potential, no charges. 293 K, 1 bar. Upper curve: a.c.f. of $\langle\omega^2(t)\omega^2(0)\rangle/\langle\omega^4(0)\rangle$, 5 × 5, no charges.

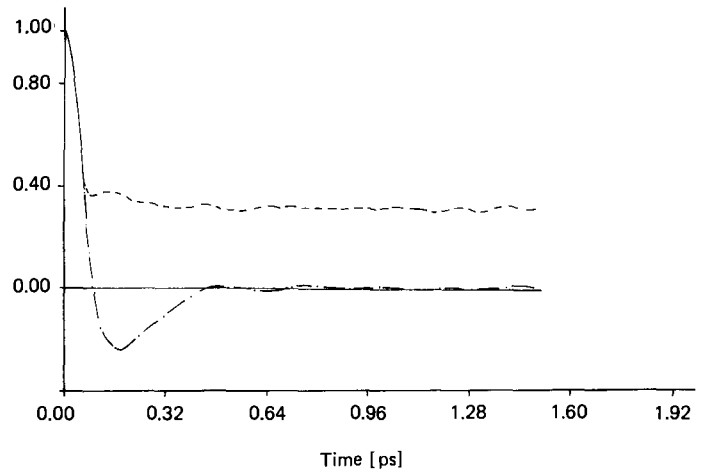

FIGURE 2.2.3.13. Lower curve: a.c.f. of molecular torque (T_q). 5 × 5 potential, no charges. 293 K, 1 bar. Upper curve: a.c.f. of $\langle T_q^2(t)T_q^2(0)\rangle/\langle T_q^4(0)\rangle$, same conditions. This curve goes to about 0.3 as $t \to \infty$.

We have concentrated on reorientational, angular-momentum, and torque a.c.f.'s. A complete description of liquid-phase dynamics involves in addition some consideration of center-of-mass translation. The most straightforward a.c.f. is that of the center-of-mass velocity and kinetic energy (Fig. 2.2.3.18). For their theoretical description these a.c.f.'s require the use of a theory based on the translational friction coefficient. This coefficient may be estimated from the area under the velocity a.c.f. of Fig. 2.2.3.18. Subsequently the phenomenological theory should produce the curves of Figs. 2.2.3.18 and 2.2.3.19. These

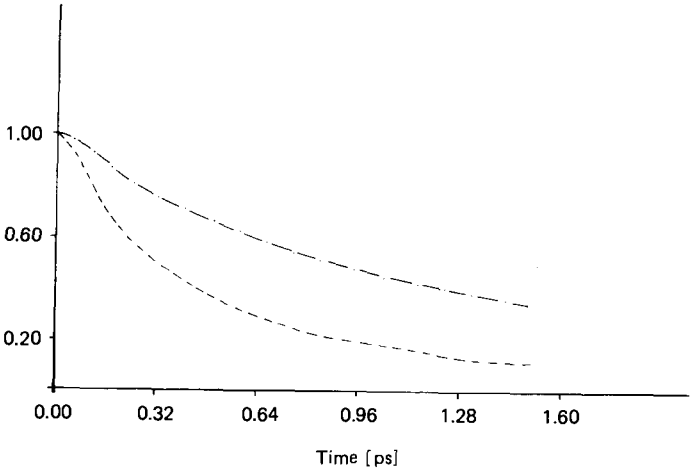

FIGURE 2.2.3.14. Upper curve: P_1 a.c.f. of $\vec{e}_A(t)$, 5 × 5, no charges, 293 K, 1 bar. Lower curve: P_2 a.c.f.

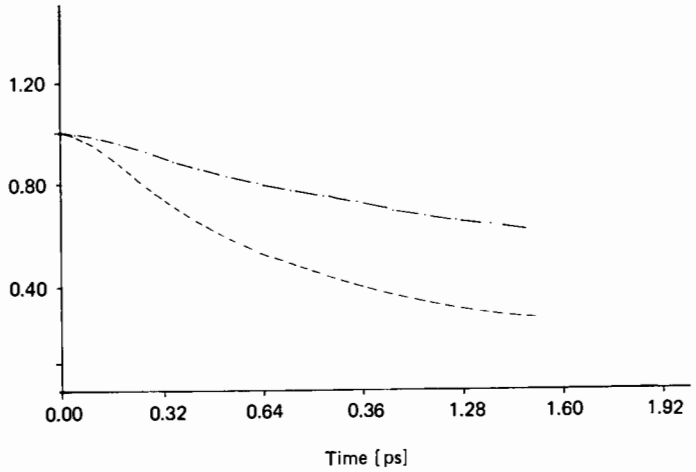

FIGURE 2.2.3.15. As in Fig. 2.2.3.14, but for $\vec{e}_B(t)$, the dipole unit vector.

are the velocity a.c.f., energy a.c.f., force a.c.f. $\langle \vec{F}(t) \cdot \vec{F}(0) \rangle / \langle F^2(0) \rangle$, and force-squared a.c.f. $\langle F^2(t) F^2(0) \rangle / \langle F^4(0) \rangle$. The last goes to a constant limit, determined by equilibrium statistics.

Having considered both the rotational and translational aspects of the 5×5 simulation results, we turn finally to a calculation of mixed autocorrelation functions. There is no clear-cut experimental method yet developed for investigating these functions directly. However, they may be simulated with little difficulty. In the laboratory (fixed) frame of reference, the mixed a.c.f. $\langle \vec{v}(0) \cdot \vec{J}(t) \rangle$ vanishes for all t because the parity of $\vec{v}$ is different from that of $\vec{J}$. Accordingly, any attempt at simulating this function produces background noise as shown in Fig. 2.2.3.20. The "mixed-energy" a.c.f. $\langle v^2(0) J^2(t) \rangle / (\langle v^2(0) \rangle \langle J^2(0) \rangle)$ exists; see Fig. 2.2.3.21, the 3×3 and 5×5 results in this case being fairly similar (Fig. 2.2.3.22). Like results are displayed for the mixed force–torque a.c.f.'s in Figs. 2.2.3.23–2.2.3.24. These a.c.f.'s do not vanish at $t = 0$.

The effects of incorporating charges at atomic sites is large enough to be of some significance. Thus an analysis based only on the Lennard-Jones potential is not sufficient. Electrical interactions must be included in order to make a

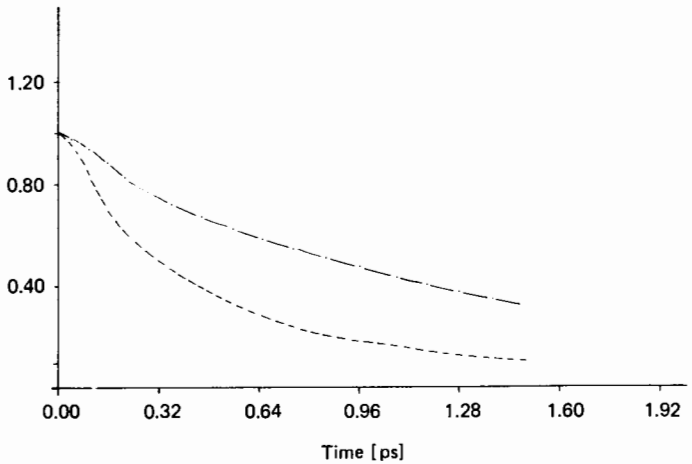

FIGURE 2.2.3.16. As in Fig. 2.2.3.14, but for $\vec{e}_C(t)$.

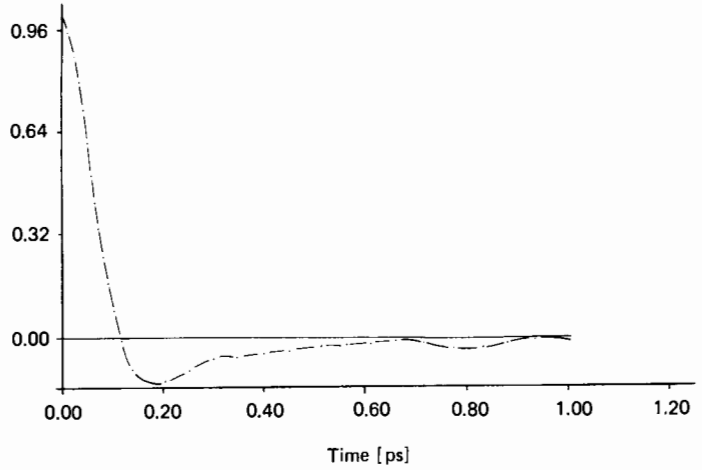

FIGURE 2.2.3.17. Rotational-velocity a.c.f. [of $\dot{\vec{e}}_A(t)$]. 5×5 potential, no charges, 293 K, 1 bar.

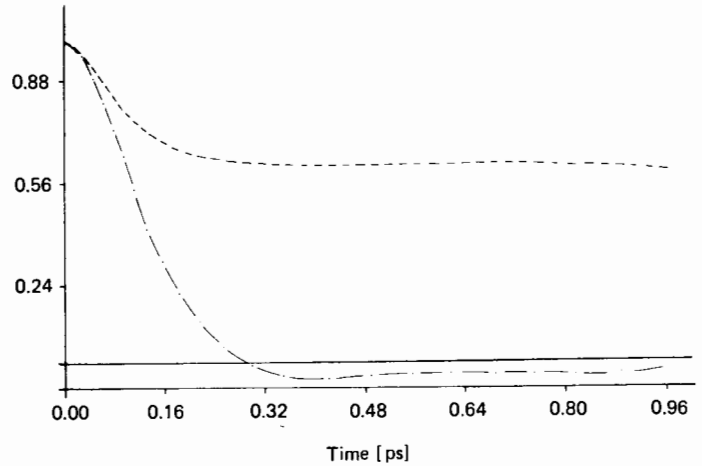

FIGURE 2.2.3.18. Lower curve: velocity a.c.f. Upper curve: kinetic-energy a.c.f. $\langle v^2(t) v^2(0) \rangle / \langle v^4(0) \rangle$, where $\vec{v}$ is the center-of-mass velocity. The horizontal line is the Gaussian limit of $\frac{3}{5}$ as $t \to \infty$. 5×5 potential, no charges, 293 K, 1 bar.

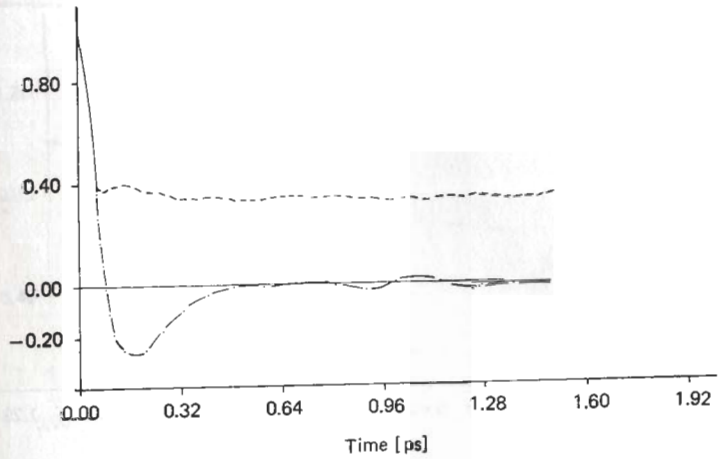

FIGURE 2.2.3.19. Lower curve: Force a.c.f. [of $\vec{F}(t)$]. 5 × 5 potential, no charges, 293 K, 1 bar. Upper curve: a.c.f. of $\langle F^2(t)F^2(0)\rangle/\langle F^4(0)\rangle$. Conditions as above. Note similarity to Fig. 2.2.3.13 upper curve).

complete analysis. The inclusion of charge–charge interaction shifts the peak of the far-infrared absorption to higher frequencies. There is a corresponding increase in the P_1 to P_4 correlation times. Hence the microwave and NMR relaxation times are increased by long-range terms of the charge–charge type etc., sometimes to a significant degree. Figures 2.2.3.25 to 2.2.3.27 are a measure of the effect of these interactions on some autocorrelation functions of CH_2Cl_2 simulated by the 3 × 3 algorithm. It is interesting to note in Fig.

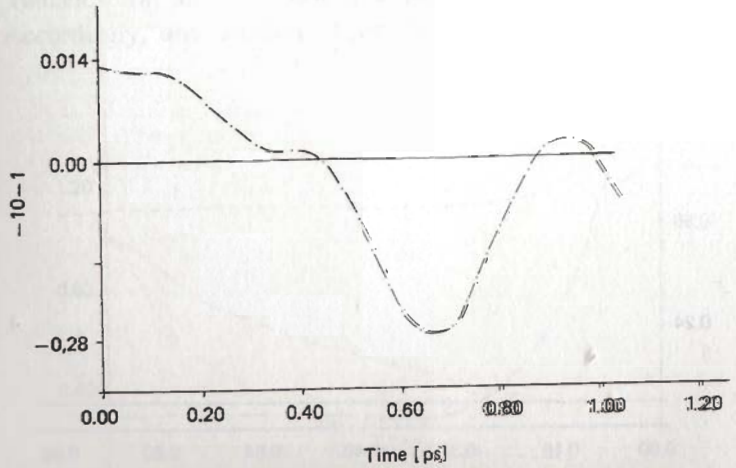

FIGURE 2.2.3.20.* Simulation of $\langle \vec{v}(t) \cdot \vec{J}(0)\rangle$, statistical noise. 5 × 5 potential, no charges, 293 K, 1 bar.

*Note abscissa is multiplied by the factor 10^{-1}.

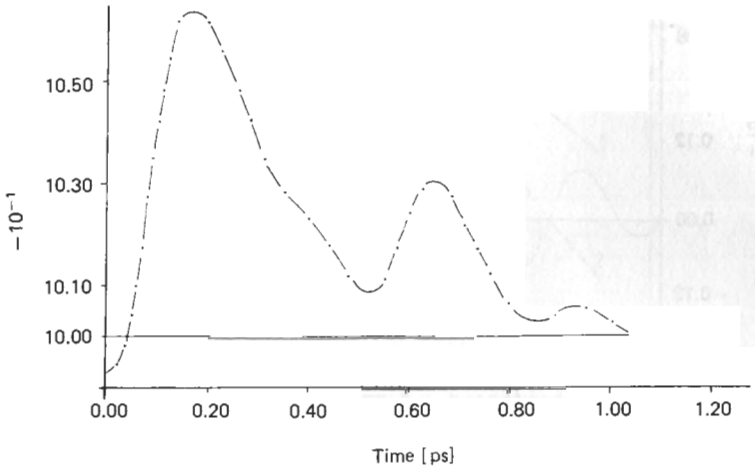

FIGURE 2.2.3.21. Mixed a.c.f. $\langle v^2(0)J^2(t)\rangle/\langle v^2(0)J^2(0)\rangle$. Genuine (except for noise in the tail), including the small deviation from unit at $t = 0$. 5 × 5 potential, no charges, 293 K, 1 bar.

2.2.3.28 that the multiparticle microscopic correlation

$$\gamma(t) = \frac{\langle \dot{\vec{e}}_{Ai}(0) \cdot \sum_{i \neq j} \dot{\vec{e}}_{Aj}(t)\rangle}{\langle \dot{\vec{e}}_{Ai}(0) \cdot \sum_{i \neq j} \dot{\vec{e}}_{Aj}(0)\rangle}$$

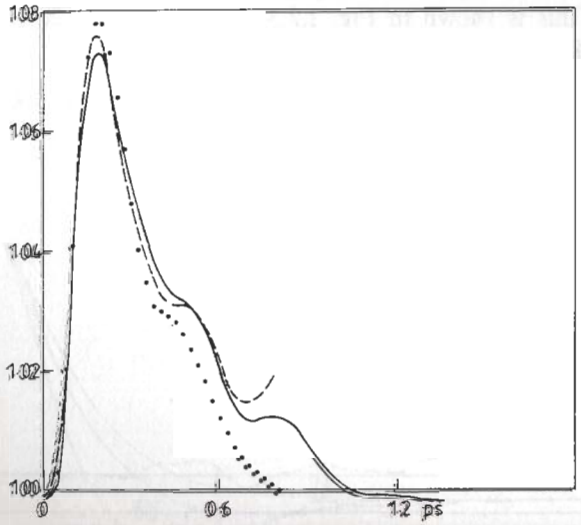

FIGURE 2.2.3.22. As in Fig. 2.2.3.21. ●: 5 × 5 algorithm, no charges, 2.5-ps running time span; solid curve: 3 × 3, no charges, 12.5-ps span; dashed curve: 3 × 3, no charges, 9-ps span. Illustrates the small $t = 0$ deviation and stable first peak.

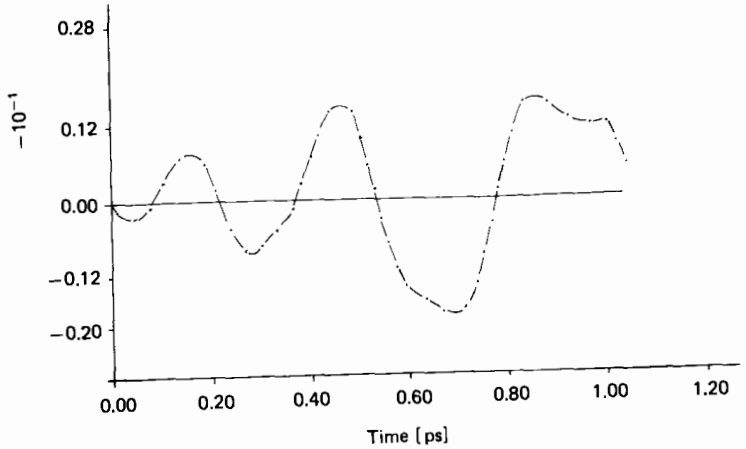

FIGURE 2.2.3.23. Mixed a.c.f. $\langle \vec{T}_q(0) \cdot \vec{F}(t) \rangle$. Statistical noise. 5 × 5, + charges, 293 K, 1 bar.

decays in a similar manner to the single-particle equivalent at 293 K. The autocorrelation and "microscopic" correlation functions do not differ significantly in structure even in the presence of electrical interactions. This provides some indication that single-particle theories of the liquid state can be used (*Molecular Dynamics*, Chapters 1–3) to provide a reasonable description of multiparticle spectra such as those in the far infrared.

The effect on the orientational a.c.f.'s of adding charges is illustrated in Figs. 2.2.3.29–2.2.3.31. The power absorption coefficient $\mathfrak{A}(\bar{\nu})$ is shifted to higher frequencies. This is shown in Fig. 2.2.3.32. Nevertheless $\mathfrak{A}$ is still below the observed peak at 80 cm^{-1}.

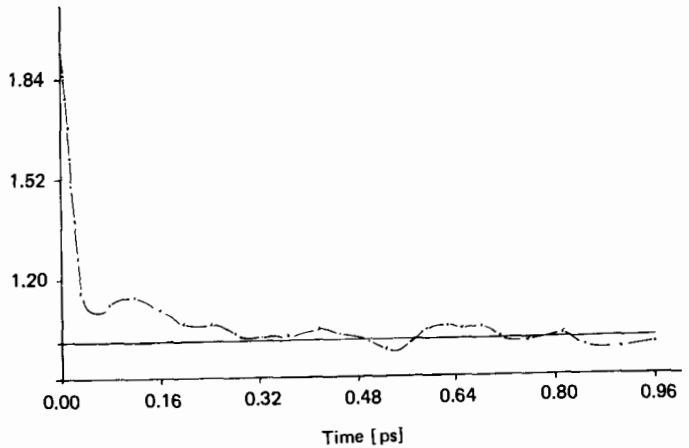

FIGURE 2.2.3.24. Mixed a.c.f. $\langle T_q^2(0)F^2(t)\rangle / \langle T_q^2(0)F^2(0)\rangle$. 5 × 5, no charges, 293 K, 1 bar. [illegible] deviation from 1 at $t = 0$. Indicative of "translation–rotation coupling."

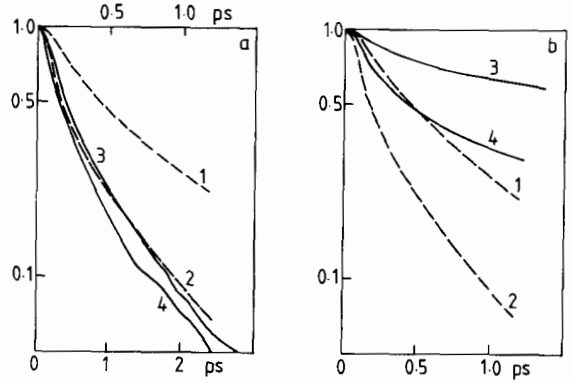

FIGURE 2.2.3.25. (a) P_1 and P_2 a.c.f.'s of $\vec{e}_A$, 3 × 3 potential. Curves 1 and 2: + charges (upper abscissa). Curves 3 and 4: no charges (lower abscissa). Both at 293 K, 1 bar. (b) Curves 1 and 2: as in (a). Curves 3 and 4: + charges, potential at 177 K, 1 bar.

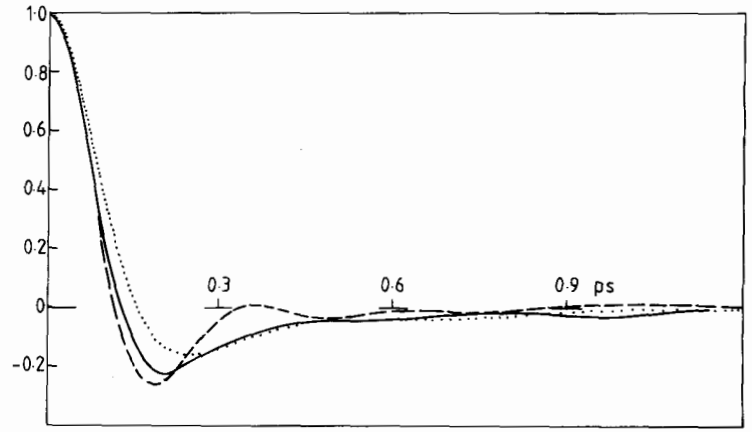

FIGURE 2.2.3.26. Rotational velocity a.c.f.'s of $\dot{\vec{e}}_A(t)$. Solid curve: 3 × 3, + charges at 293 K, 1 bar; dashed curve: 3 × 3, + charges at 177 K, 1 bar; dotted curve: 3 × 3, no charges at 293 K, 1 bar.

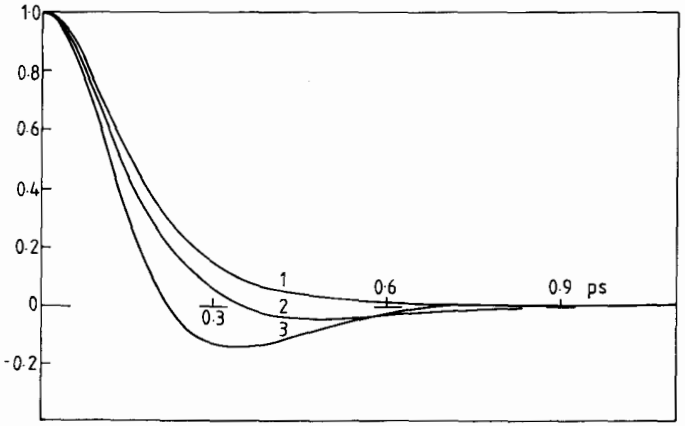

FIGURE 2.2.3.27. Comparison of angular-momentum a.c.f.'s. Curve 1: 3 × 3, no charges, 293 K,

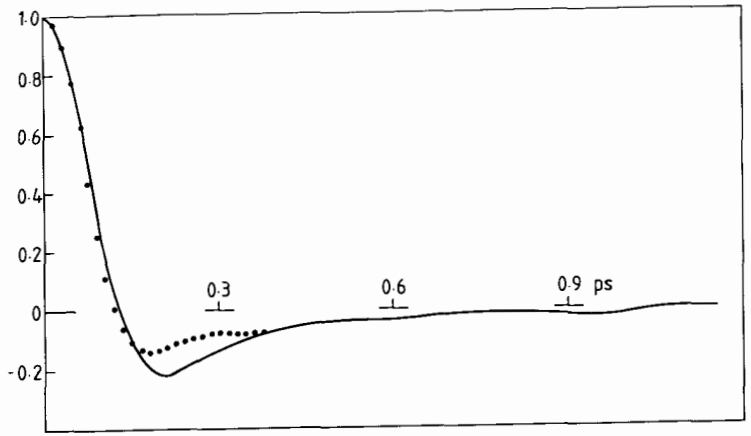

FIGURE 2.2.3.28. Solid curve: a.c.f. of $\dot{\vec{e}}_A(t)$, 3 × 3, + charges, 293 K, 1 bar. ●: $\langle \dot{\vec{e}}_{Ai}(0) \cdot \Sigma_j \dot{\vec{e}}_{Aj}(t) \rangle / \langle \dot{\vec{e}}_{Ai}(0) \cdot \Sigma_j \dot{\vec{e}}_{Aj}(0) \rangle$ computed for a spherical subsample containing two or three molecules.

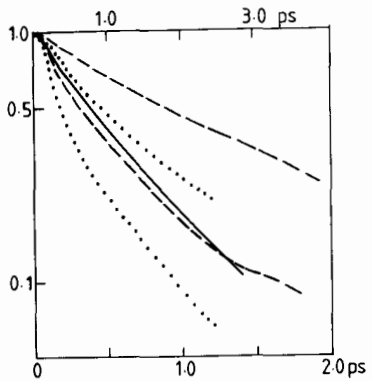

FIGURE 2.2.3.29. Solid curve: P_1 a.c.f. of $\vec{e}_A$, 5 × 5, no charges, 293 K, 1 bar (upper abscissa). Dashed curves: P_1 and P_2 a.c.f.'s of $\vec{e}_A$, 5 × 5, + charges, 293 K, 1 bar (lower abscissa). Dotted curves: P_1 and P_2 a.c.f.'s of $\vec{e}_A$, 3 × 3, + charges, 293 K, 1 bar (lower abscissa).

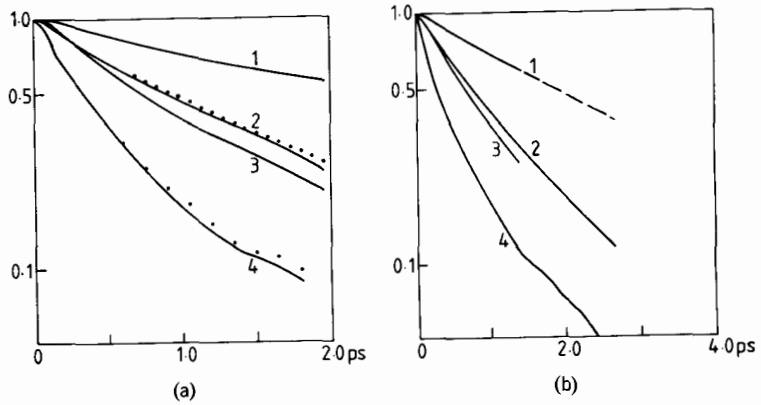

FIGURE 2.2.3.30. (a) Anisotropy of rotational diffusion: 5 × 5 potential, + charges, 293 K, 1 bar. Curve 1: P_1 a.c.f. of $\vec{e}_B$; curve 2: P_1 a.c.f. of $\vec{e}_A$; curve 3: P_2 a.c.f. of $\vec{e}_B$ curve 4: P_2 a.c.f. of $\vec{e}_B$ (solid curve) and of $\vec{e}_C$ (dotted curve). (b) As in (a), but no charges. P_1 and P_2 of $\vec{e}_C$ are not shown, being very similar to those of $\vec{e}$.

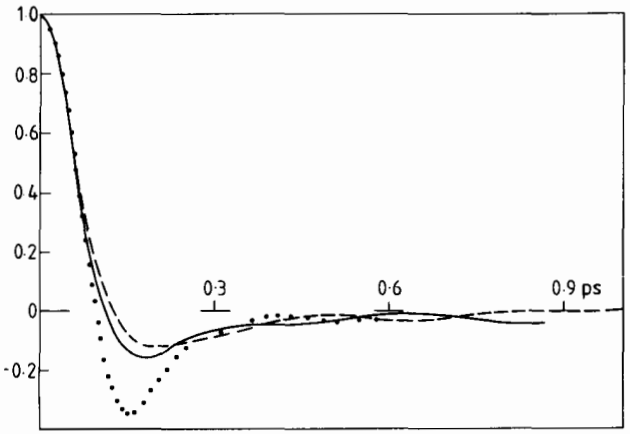

FIGURE 2.2.3.31. Rotational-velocity a.c.f.'s [of $\dot{\vec{e}}_A(t)$]. Dashed curve: 5 × 5, no charges, 293 K, 1 bar. Solid curve: 5 × 5, with charges, 293 K, 1 bar. Dotted curve: computed from far-infrared data on pure liquid CH_2Cl_2.

2.2.4. Summary of the CH_2Cl_2 Computer Simulation

We have just described how molecular-dynamics simulation is used to transform intermolecular-potential parameters such as σ and ϵ/k directly into theoretical correlation functions. Further these may be converted via Fourier

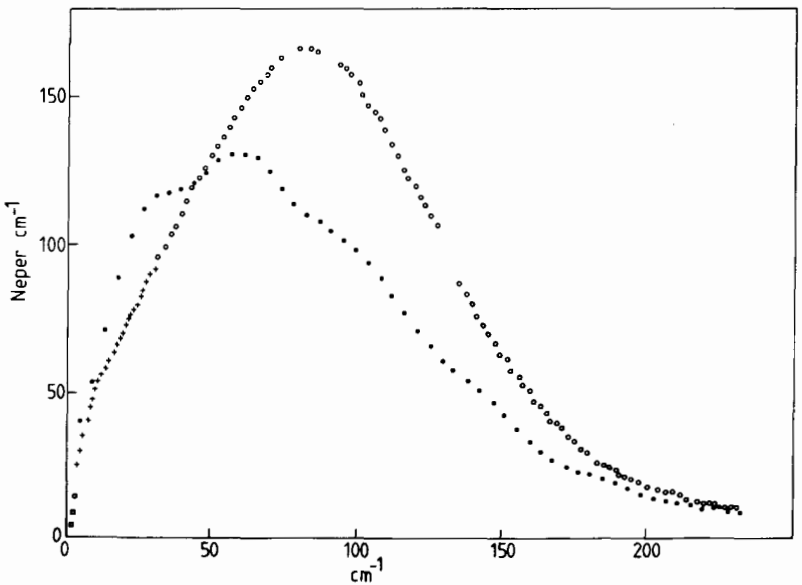

FIGURE 2.2.3.32. As in Fig. 2.2.3.1 except that ● denote values obtained by Fourier transformation of the rotational-velocity a.c.f. [of $\dot{\vec{e}}_A(t)$] for the 5 × 5 +charges potential. The Fourier transform is noisy due to artifacts introduced by the long tail of the a.c.f.

transformation into theoretical spectra of the liquid state. As computer power and accessibility increase, this will become routine during the growth of the Delta Project. It is therefore apparent that a multitechnique approach to liquid-state spectroscopy must also become routine to deal with the catholicity of the new hypotheses embodied in computer simulation. The liquid should be investigated at a given state point from as many different viewpoints as possible. These state points should cover the complete range from triple point to critical point, using pressure as well as temperature and viscosity as variables.

The whole range of real and simulated spectra should be used with one aim; namely the improvement of our understanding of the way in which molecules interact in the liquid state of matter. Thus it is important to restructure the molecular dynamics algorithm so that the results of *ab initio* calculations (van der Avoird et al., 1980) can be used in the force loops of algorithms such as TETRAH. The model potentials should be tried out on useful thermodynamic data such as those on the second dielectric virial coefficient B_ϵ and third pressure virial coefficient C_p. Frequently model potentials, which seem to work well in some areas, produce the wrong sign for B_ϵ. In contrast, atom–atom plus-charge models appear to work better than *ab initio* calculations. This was noted by van der Avoird et al. (1980).

In Section 2.2.3, we made a limited study of the dynamic properties of liquid CH_2Cl_2 with two different atom–atom potentials. These potentials could be improved if the necessary B_ϵ data were available over a wide temperature range. The zero-to-terahertz range of frequencies is also a sensitive test of the way molecules interact. It is known, for example, that the spectrum of CH_2Cl_2 changes dramatically in dilute, supercooled decalin solution, encompassing an enormous range of frequency—in fact, a dozen decades. This is mentioned in Chapter 1.

The effect of adding charges to the core 5×5 (and 3×3) atom–atom potentials is significant. Using center-to-mass-to-center-of-mass cutoff, it appears that the long range of the charge–charge interaction does not pose any difficulty, even for as few as 108 molecules. We require more molecules than 108 and longer simulation runs for a more accurate calculation of many-body correlation functions (used in the interpretation of Brillouin and acoustic spectra). The calculation of cross correlations in Section 2.2.3 was restricted to a microscopic sphere of about 8-Å radius. This contains, on average, only two or three molecules. In order to improve these calculations, we hope to incorporate, during Delta, the effects of polarizability, intramolecular vibration, and reaction fields.

2.3. THE INTERACTION OF ROTATION AND TRANSLATION IN CH_2Cl_2 AND CH_3CN

One of the most interesting problems of the liquid state of matter is that of understanding the mutual effects of rotation and translation. It is known that

rotational motion is affected by translational motion. However, the problem of unraveling the relevant autocorrelation functions has only recently been approached correctly. We study the rotational–translational autocorrelation functions of interest in a *moving frame of reference*, fixed in the molecule.

If, as an example, we take the molecular center-of-mass linear velocity $\vec{v}$ and the angular velocity $\vec{\omega}$ (or angular momentum $\vec{J}$), there are symmetry theorems (Evans et al., 1982) which do not allow $\langle \vec{v}(0) \cdot \vec{J}(t) \rangle$ to exist in the laboratory frame. However, in a moving frame of reference, these a.c.f.'s exist. The various components of the matrix $\langle \mathbf{v}(0)\mathbf{J}^T(t) \rangle$ may be used to build up a picture of the rotation–translation interaction. Up to nine elements of this a.c.f., depending on the molecular symmetry, may be simulated on a computer using the technique of molecular dynamics (described in Section 2.1). If the molecule under consideration is optically active, all nine elements are different and provide us with a complete description of the molecular behavior during the first picoseconds of rotational–translational motion.

In the moving frame of reference, the three components of $\langle \vec{J}(t) \cdot \vec{J}(0) \rangle$ [or alternatively $\langle \vec{v}(t) \cdot \vec{v}(0) \rangle$] no longer possess identical time dependences. One finds that the components of the velocity a.c.f. are initially anisotropic, but at long times are isotropic in a moving frame of reference fixed in the molecule's principal moment-of-inertia system. This means that the classical approach to molecular diffusion, based on considerations in the *laboratory* frame, should be revised to operate in the *moving* frame. In this frame, molecular-symmetry effects come into play. Later on, as an example, we shall rewrite the appropriate Langevin equation in the moving frame of reference. Molecular properties such as the dipole moment and polarizability can be expressed in a moving frame using spherical tensors. The coordinates of the spherical tensor of rank l are the spherical harmonics $Y_m^l(\Omega)$ $(m = -l, \ldots, l)$. The spherical angles $\Omega = (\theta, \phi)$ depend on the tensorial property of the molecule in which we are interested. Under rotation the spherical tensors transform according to the irreducible representations of the rotational group O_3^+. Transformation from moving to laboratory frame would result in rotation–translation coupling being expressed in terms of the spherical harmonics, $Y_m^l[\Omega(t)]$. This is true even for the center-of-mass velocity $\vec{v}(t)$, due to the effect of rotation upon translation. In what follows, we describe the results of machine experiments on CH_2Cl_2 and CH_3CN.

2.3.1. Symmetry Properties in Fixed and Moving Frames of Reference

When dealing with the collective motions of molecules, the interaction of rotational and translational modes of motion makes use of symmetry properties in the laboratory frame. Ailawadi, Berne, and Foster (1971) have dealt with these in detail. The symmetry theorems are summarized by Berne and Pecora (1976). These theorems place severe constraints on mixed a.c.f.'s of rotation and translation for a single molecule. In particular, the mixed a.c.f.'s $\langle \vec{v}(t) \cdot \vec{J}(0) \rangle$ (or the elements of $\langle \mathbf{v}(t)\mathbf{J}^T(0) \rangle$) vanish for all t. Here $\vec{v}$ is the center-of-mass linear velocity and $\vec{J}$ the molecular angular momentum. Chiral

molecules and molecules subjected to an uniaxial magnetic field in the laboratory frame may be exceptions. The direct influence of rotation on translation or vice versa cannot be observed using these a.c.f.'s.

However, we know that in the liquid state molecular translation *does* affect rotation (Evans et al., 1982). Any spectral function labeled as rotational in origin is rotational–translational. Thus parameters such as the friction coefficient contain both rotational and translational effects. In consequence, dielectric data such as those encountered in zero-to-terahertz spectroscopy cannot be interpreted satisfactorily without first finding a theoretical means of unraveling the information contained in the friction coefficient.

There are two well-developed methods of proceeding, using phenomenological (i.e. Debye-type) theory and kinetic theory. Using the first approach, Condiff and Dahler (1966) have arrived at relations similar to those of Onsager and Casimir. However, since the whole of this calculation is carried out in the laboratory frame, the final results conflict with the symmetry requirement that $\langle \mathbf{v}(0)\mathbf{J}^T(t)\rangle$ must vanish for all t. These authors also developed an approach based on kinetic theory which is very complicated and has no clear outcome. Condiff and Dahler's (1966) methods might be applicable to chiral molecules. They might also be used to study the return to equilibrium after switching off an intense magnetic field. The sample is monitored by a weak measuring field.

Lately, several authors have treated the multiparticle problem theoretically in the laboratory frame. A paper by G. T. Evans (1978) considers the motion of a propeller-shaped molecule on the basis of rotational–translational Fokker–Planck equations. Evans concludes that rotational–translational correlation functions under consideration vanish for most molecular symmetries in the laboratory frame. Deutch and Wolynes (1977) have considered the rotational–translational nature of the phenomenological friction coefficient, using hydrodynamic theory based on the Oseen tensors. They also used many-particle equations of motion. The classical theory of Debye just considers one rotating dipole having spherical symmetry, the effect of all the interactions being modeled as Brownian movement, (Hill et al., 1968).

One should note that although elements of $\langle \mathbf{v}(0)\mathbf{J}^T(t)\rangle$ vanish for all t in the static laboratory frame, they *do not* in a moving frame of reference fixed in the molecule. For convenience this frame (1, 2, 3) may be taken as that coinciding with the three principal axes of inertia. On studying the behavior of $\langle \vec{v}(t)\cdot\vec{v}(0)\rangle$, $\langle \vec{J}(t)\cdot\vec{J}(0)\rangle$, and $\langle \mathbf{v}(0)\mathbf{J}^T(t)\rangle$ in this moving frame (1, 2, 3), we can derive, by computer simulation, new information about the behavior in the laboratory frame. We may then attempt to describe these computer-simulation results with an analytical approach. Such a theory would essentially describe the numerical information from the computer simulation by means of friction coefficients (or a series of memory functions) *defined with respect to the moving frame of reference*. We believe this idea to be new. The new theory must obey the laboratory-frame constraint $\langle \vec{v}(t)\cdot\vec{J}(0)\rangle = 0$ for all t.

Now, the new theoretical equations for $\langle \vec{J}(t)\cdot\vec{J}(0)\rangle$ (and thereby for dielectric and far-infrared spectroscopy) involve rotational–translational friction coefficients (say, γ_{rt}), as well as translational–rotational (γ_{tr}), translational (γ_t) and rotational (γ_r) coefficients. They are defined initially for the moving frame. They are then transferred back into the laboratory frame. We may put a value (in terahertz units) on each element of the matrix $\boldsymbol{\gamma}$, provided we have enough simulated a.c.f.'s. We then compare the theoretical and experimental rotational–translational zero-to-terahertz spectra. Grigolini et al. (1981) have developed a theoretical method and numerical algorithm for dealing with the evolution of $\boldsymbol{\gamma}$ as a series of memory functions. They use a form of the Mori continued fraction.

We illustrate the interaction of experimental observation, computer simulation, and analytical theory, We use as examples the European Molecular Liquids Group Pilot Project molecules (Evans et al., 1982) dichloromethane (CH_2Cl_2, a C_{2v}-symmetry asymmetric top) and acetonitrile (CH_3CN, a C_{3v}-symmetry symmetric top).

2.3.2. The Frame Transformation and Moving-Frame A.C.F.

Vector quantities such as $\vec{v}$, $\vec{J}$, $\vec{F}$ (force), and $\vec{T}$ (torque on a molecule) may be defined in either the laboratory frame or the moving frame. The components of $\vec{v}$ in the laboratory frame are v_x, v_y, v_z; in the moving frame, v_1, v_2, v_3. We define three unit vectors $\vec{e}_1, \vec{e}_2, \vec{e}_3$ with respect to the frame (1, 2, 3). The velocity components are then related by

$$\begin{aligned} v_1 &= v_x e_{1x} + v_y e_{1y} + v_z e_{1z} \\ v_2 &= v_x e_{2x} + v_y e_{2y} + v_z e_{2z} \\ v_3 &= v_x e_{3x} + v_y e_{3y} + v_z e_{3z} \end{aligned} \qquad (2.3.2.1)$$

In CH_3CN $\vec{e}_1 = \vec{e}_2$, and in CH_2Cl_2 $\vec{e}_2 \simeq \vec{e}_3$, so that $v_1 = v_2$ for CH_3CN and $v_2 \simeq v_3$ for CH_2Cl_2. In equation (2.1) e_{1x} is the x component of $\vec{e}_1$ in the laboratory frame, and so on.

Having made the transformation [equation (2.3.2.1)] into the moving frame (Fig. 2.3.2.1) for each vector $\vec{v}$, $\vec{J}$, $\vec{F}$, and $\vec{T}_q$, we evaluate the correlation functions $\langle \vec{v}(t)\cdot\vec{v}(0)\rangle_m$, $\langle \vec{J}(t)\cdot\vec{J}(0)\rangle_m$, $\langle \mathbf{F}(t)\mathbf{T}_q^T\rangle_m$, $\langle \vec{F}(t)\cdot\vec{F}(0)\rangle_m$, and $\langle \vec{T}_q(t)\cdot\vec{T}_q(0)\rangle$. Here $\langle\ \rangle_m$ denotes a running time average over vector components defined with respect to the moving frame of reference (1, 2, 3). An analytical description of these functions is suggested in the next section. It is possible to see that all the elements of $\langle \mathbf{v}(t)\mathbf{J}^T(0)\rangle$ and $\langle \mathbf{F}(t)\mathbf{T}_q^T(0)\rangle$ vanish except the off-diagonal elements $\langle v_1(t)J_2(0)\rangle$ and $\langle v_2(t)J_1(0)\rangle$. This is done by applying parity-reversal symmetry for CH_2Cl_2 (Berne and Pecora, 1976). Other elements will exist for CH_3CN. They are very small in magnitude compared with the two listed above. The nonvanishing elements are mirror images of each other in CH_3CN but are not symmetric in CH_2Cl_2 (Fig. 2.3.2.2). We have made convenient use of the definition

$$\langle 2,1\rangle_m = \frac{\langle v_2(t)J_1(0)\rangle_m + \langle v_2(0)J_1(t)\rangle_m}{2\langle v_2^2(0)\rangle_m^{1/2}\langle J_1^2(0)\rangle_m^{1/2}} \qquad (2.3.2.2)$$

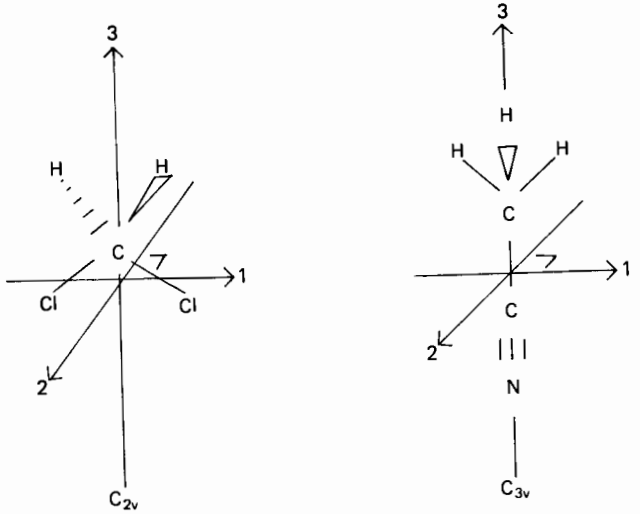

FIGURE 2.3.2.1. Description of the moving frames of reference for CH_2Cl_2 and CH_3CN.

and similarly for the other elements. For a stationary process we should have $\langle v_2(t)J_1(0)\rangle_m = \langle v_2(0)J_1(t)\rangle_m$, and any residual difference in the computer simulation is due to noise. In equation (2.3.2.2), we have simply taken the average to improve the quality of the a.c.f.'s $\langle 2,1\rangle_m$. The normalization in equation (2.3.2.2) allows us to compare directly the results from CH_2Cl_2 and CH_3CN at the same state point (293 K, 1 bar).

The $\langle 1,2\rangle_m$ a.c.f. in CH_2Cl_2 [Fig. 2.3.2.2(b)] peaks at about $+0.02$, and the $\langle 2,1\rangle_m$ at just below $+0.02$. The equivalent numbers in CH_3CN [Fig. 2.3.2.2(a)] are -0.23 and $+0.23$ respectively. One must remember that we are dealing here with molecules of high symmetry (C_{3v} and C_{2v}). In low-symmetry (e.g. chiral) molecules, all nine elements of $\langle \mathbf{v}(t)\mathbf{J}^T(0)\rangle$ may exist. Liquid crystals are often composed of chiral or low-symmetry molecules. It is probable that their peculiar properties may be described in terms of the elements $\langle\ \rangle_m$. An analytical theory for $\langle\ \rangle_m$ would carry this description into the laboratory frame and provide us with some spectra. The theory may provide us with more than one dielectric-loss peak in the manner of the director-potential theory now used. Figure 2.3.2.3 carries the same information in terms of normalized elements of $\langle \mathbf{F}(t)\mathbf{T}_q^T(0)\rangle$. These do not vanish as the corresponding normalized $\langle \mathbf{v}(t)\mathbf{J}^T(0)\rangle$ elements do. For force (torque a.c.f.'s at $t = 0$), we have for CH_2Cl_2 $\langle 1,2\rangle_m = -0.07$, $\langle 2,1\rangle_m = +0.33$. For CH_3CN, $\langle 1,2\rangle_m = -0.75$, $\langle 2,1\rangle_m = 0.75$. In CH_3CN the elements are symmetrical (i.e. mirror images).

Having studied the mixed a.c.f.'s, the moving-frame velocity and angular-momentum a.c.f.'s can be described. These are $\langle \vec{v}(t)\cdot\vec{v}(0)\rangle$ and $\langle \vec{J}(t)\cdot\vec{J}(0)\rangle$. The three components of each of these a.c.f.'s need no longer be isotropic in the moving frame as opposed to the usual laboratory frame of reference. This appears to be the first direct description of these. Diffusional anisotropy in the laboratory frame has often been described before, however. In Fig 2.3.2.4 we

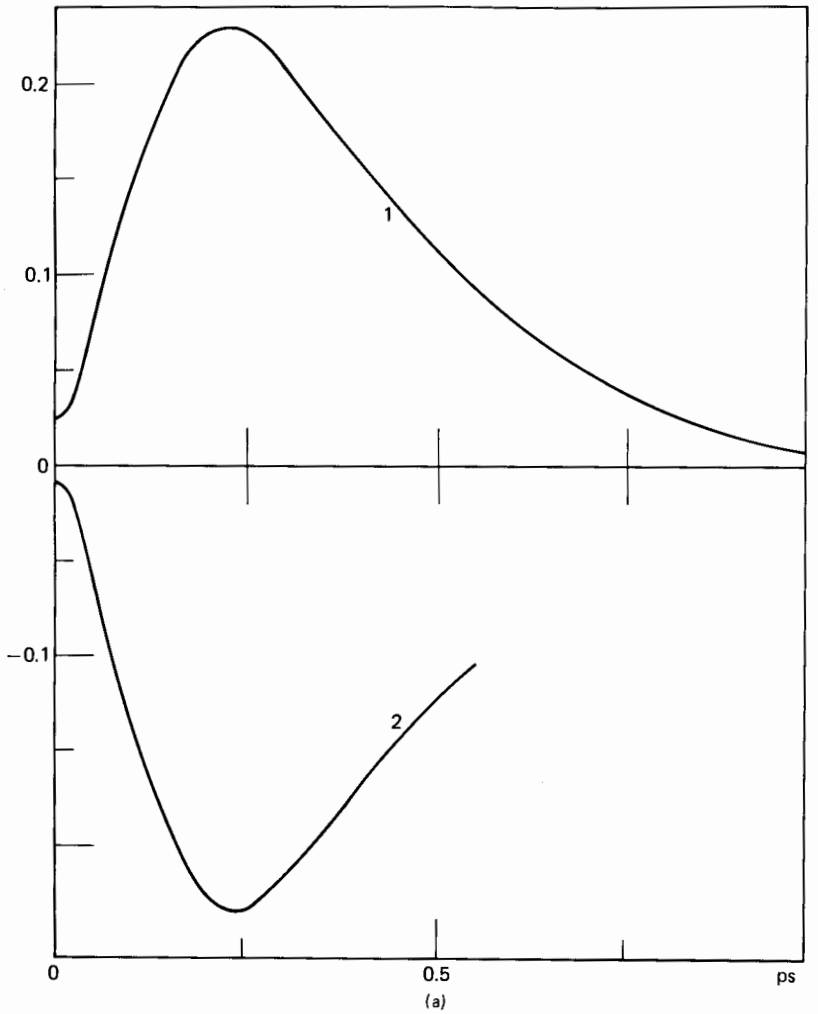

FIGURE 2.3.2.2. Moving-frame mixed autocorrelation functions. (a) For CH_3CN. Curve 1:

$$\langle 2,1\rangle_m = \frac{\langle v_2(t)J_1(0)\rangle_m + \langle v_2(0)J_1(t)\rangle_m}{2\langle v_2^2(0)\rangle_m^{1/2}\langle J_1^2(0)\rangle_m^{1/2}}$$

curve 2:

$$\langle 1,2\rangle_m = \frac{\langle v_1(t)J_2(0)\rangle_m + \langle v_1(0)J_2(t)\rangle_m}{2\langle v_1^2(0)\rangle_m^{1/2}\langle J_2^2(0)\rangle_m^{1/2}}$$

(b) for CH_2Cl_2. Curve 1: $\langle 2,1\rangle_m$; curve 2: $\langle 1,2\rangle_m$.

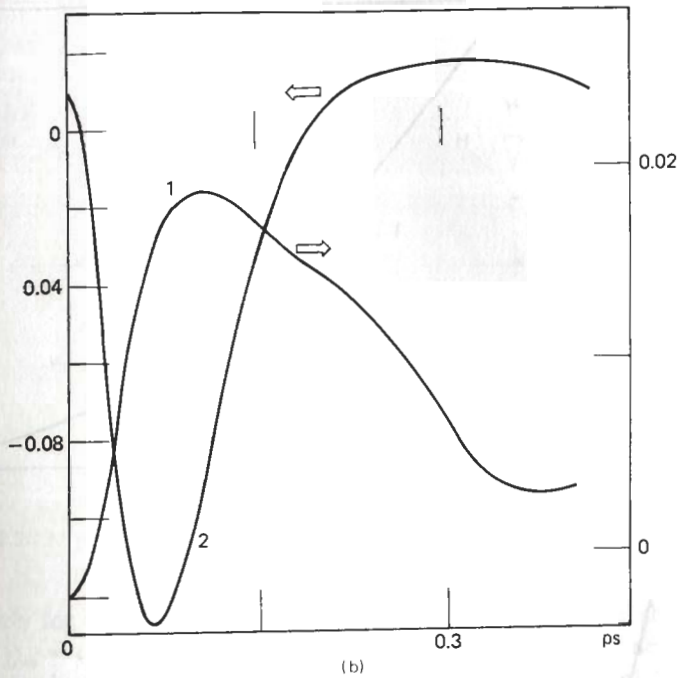

FIGURE 2.3.2.2. *Continued*

describe the $\langle v_1(t)v_1(0)\rangle$ and $\langle v_2(t)v_2(0)\rangle$ a.c.f.'s for CH_2Cl_2, and in Fig. 2.3.2.5 the $\langle v_1(t)v_1(0)\rangle$ and $\langle v_2(t)v_2(0)\rangle$ a.c.f.'s for CH_3CN. Both moving-frame a.c.f.'s behave in such a manner that at intermediate times two elements decay at different rates. At long times the two components behave isotropically, however. The maximum difference between the two component a.c.f.'s for each coincides with the maximum in the mixed a.c.f.'s described in Fig. 2.3.2.2. In CH_3CN this is also true of the molecule-frame components of $\langle \vec{J}(t)\cdot\vec{J}(0)\rangle$ (Fig. 2.3.2.6). Translation–rotation coupling therefore appears to be operative primarily at short times. The secondary effects are longer-lived, however. The mixed a.c.f.'s are finite for a long time after $\{\langle v_3^2(0)\rangle_m^{-1}\langle v_3(t)v_3(0)\rangle_m\}$ and $\langle v_1(t)v_1(0)\rangle/\langle v_1^2(0)\rangle_m$ have come together in the moving frame.

We describe finally some kinetic-energy autocorrelation functions which are invariant from frame to frame. This happens because the correlation variates are scalars. Therefore this type of a.c.f. exists in the laboratory frame (Quentrec and Brot, 1975). In Fig. 2.3.2.7 we illustrate the mixed kinetic-energy a.c.f.'s $[\langle v_i^2(0)J_j^2(t)\rangle + \langle v_i^2(t)J_j^2(0)\rangle]/[2\langle v_i^2(0)\rangle\langle J_j^2(0)\rangle]$, where $i, j = 1,2,3$ in any combination. The theory should reproduce their behavior. Component a.c.f.'s such as $\langle v_2^2(t)v_2^2(0)\rangle/\langle v_2^2(0)\rangle$ and $\langle v_3^2(t)v_3^2(0)\rangle/\langle v_3^2(0)\rangle$ are anisotropic in the *laboratory frame*.

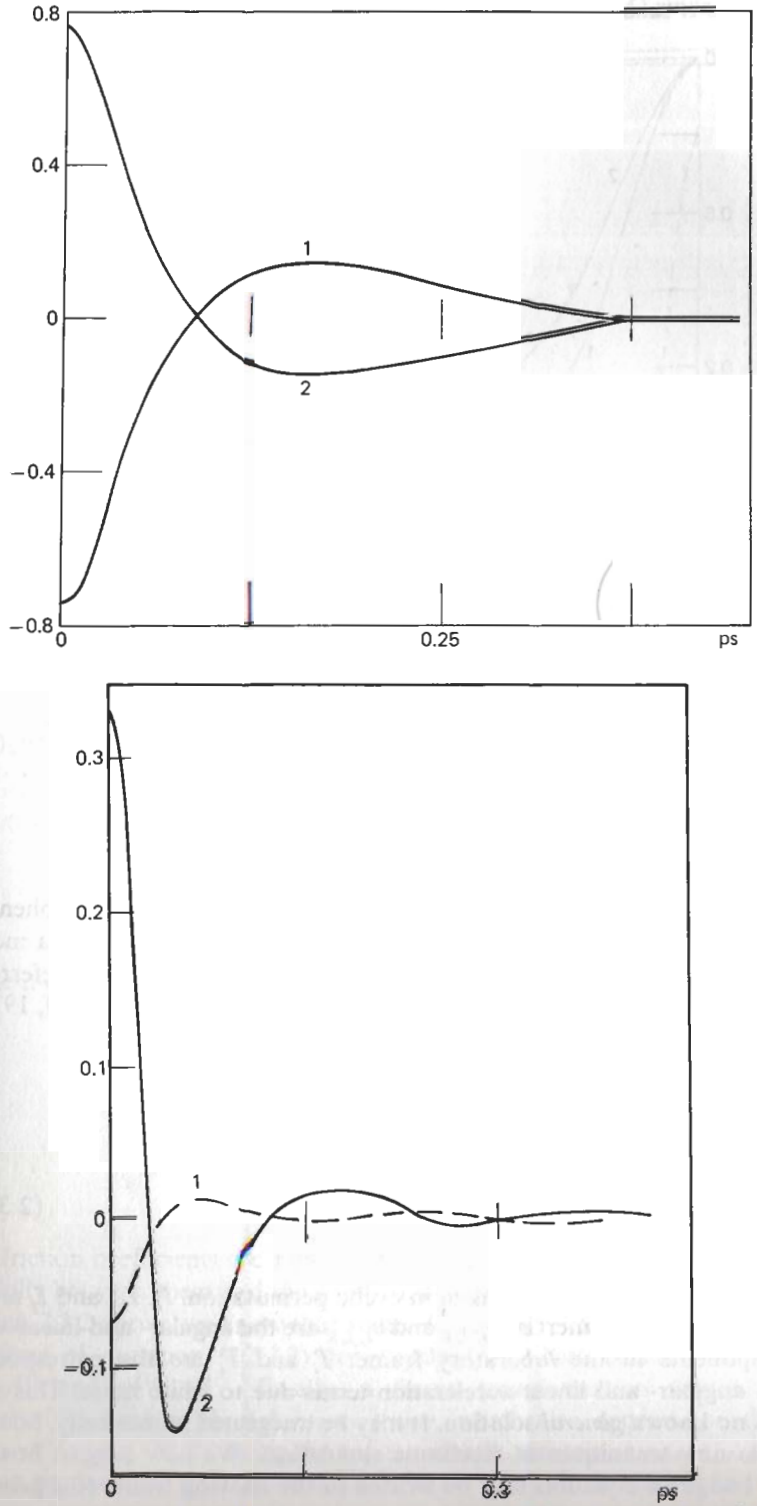

FIGURE 2.3.2.3. Force–torque a.c.f.'s in the moving frame: upper, CH_3CN; lower, CH_2Cl_2

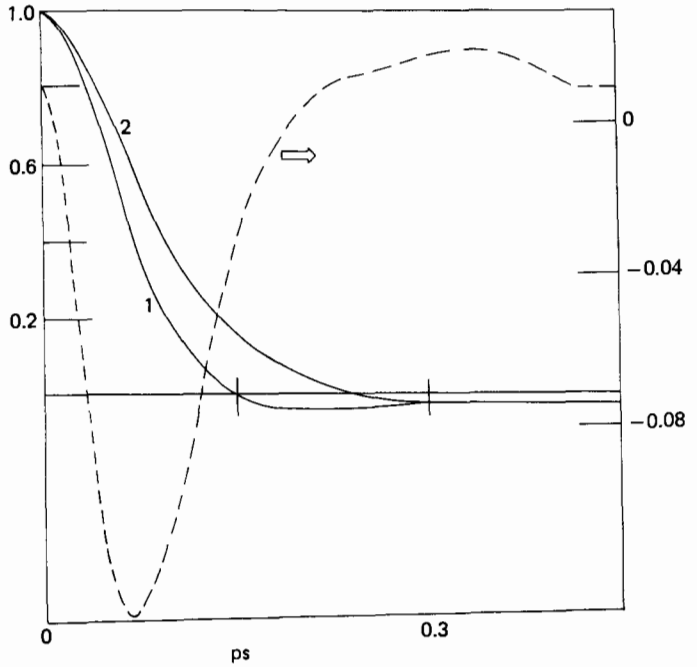

FIGURE 2.3.2.4. Curve 1: $\langle v_1(t)v_1(0)\rangle_m/\langle v_1^2(0)\rangle_m$ for CH_2Cl_2. Curve 2: $\langle v_2(t)v_2(0)\rangle_m/\langle v_2^2(0)\rangle_m$. Dashed curve: (1, 2) element of the mixed a.c.f. [Fig. 2.3.2.2(b)].

2.3.3. Theoretical Treatment of A.C.F.'s

We are now concerned with rewriting the familiar equations of the phenomenological theory of molecular diffusion so that they can be used in a moving frame of reference. The equations of motion of an asymmetric top, referred to a body-fixed frame, are (Quentrec and Brot, 1975; Hwang and Freed, 1975)

$$\dot{\omega}_i = \frac{I_i - I_k}{I_i}\omega_i\omega_k - \sum_{l=1}^{3}\left(\beta_{il}^{(r)}\omega_l + \beta_{il}^{(rt)}v_l\right) + T_i(t)$$

$$\dot{v}_i = -\sum_{l=1}^{3}\left(\beta_{il}^{(t)}v_l + \beta_{il}^{(tr)}\omega_l\right) + F_i(t) \qquad (2.3.3.1)$$

The subscripts i, j, and k are taken in cyclic permutation. I_i, I_k, and I_j are the principal moments of inertia, $\omega_{i,j,k}$ and $v_{i,j,k}$ are the angular- and linear-velocity components in the laboratory frame. T_i and F_i are the corresponding random angular- and linear-acceleration terms due to white noise. This equation has no known *general* solution. It may be integrated numerically, however, using the new techniques of stochastic simulation. We now suggest how this type of Langevin equation may be written in the moving frame (the principal

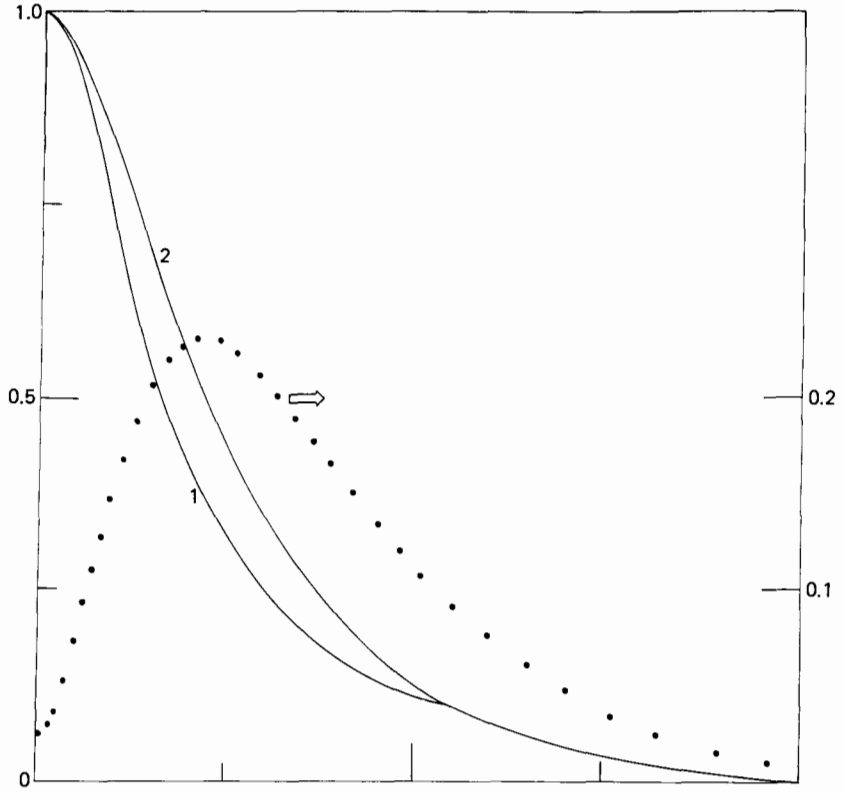

FIGURE 2.3.2.5. As in Fig. 2.3.2.4: acetonitvile.

moment-of-inertia axis frame):

$$\dot{\omega}_i = \frac{I_i - I_k}{I_i}\omega_j\omega_k - \sum_{l=1}^{3}\left(\gamma_{il}^{(r)}\omega_l + \gamma_{il}^{(rt)}v_l\right) + T_i(t)$$

$$\dot{v}_i = v_j\omega_k - \omega_j v_k - \sum_{l=1}^{3}\left(\gamma_{il}^{(t)}v_l + \gamma_{il}^{(tr)}\omega_l\right) + F_i(t) \qquad (2.3.3.2)$$

The friction coefficients are now written as γ. This is in order to differentiate carefully between them and the fixed-frame coefficients β. Using the results of Section 2.3.2 above, we know that some elements $\gamma^{(tr)}$ and $\gamma^{(rt)}$ are finite. The solutions of equation (2.3.3.2) for $\langle v_i(0)v_i(t)\rangle_m$ *both contain the elements* $\gamma^{(r)}, \gamma^{(t)}$ and $\gamma^{(tr)}, \gamma^{(rt)}$. Finally, a frame transformation would give us $\langle\omega_i(t)\omega_i(0)\rangle$ *back in the laboratory frame*, which also depends on the cross terms $\gamma^{(tr)}$ and $\gamma^{(rt)}$. By using the fundamental kinematic equation $\dot{\vec{u}} = \vec{\omega}\times\vec{u}$, we can produce the orientational a.c.f. $\langle\vec{u}(t)\cdot\vec{u}(0)\rangle$ (in the laboratory frame).

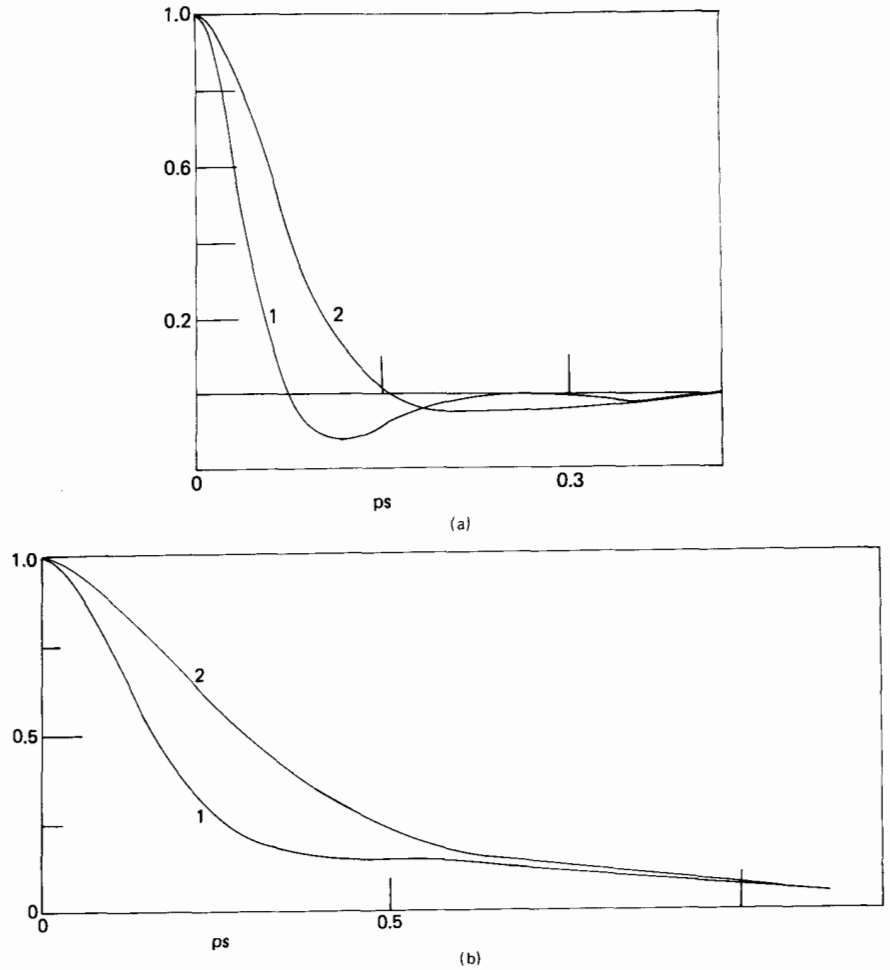

FIGURE 2.3.2.6. As in Fig. 2.3.2.4, but showing angular-momentum components in the moving frame (a) for CH_2Cl_2, (b) for CH_3CN.

We can then calculate the dielectric and far-infrared spectra and also the Raman, NMR, and Rayleigh-scattering bandshapes. These depend essentially on a high-order correlation function of $\vec{u}$.

There is no known analytical solution to equation (2.3.3.2). It may be solved numerically using the stochastic-simulation method. We may attempt to match the computer-simulation results by varying the elements. This will give us numerical values of the γ elements in terahertz units. The relative sizes of the γ elements are a quantitative indication of the influence of rotation on translation and vice versa.

Equation (2.3.3.2) should be tested in a coordinated manner against experimental results from different techniques (e.g. the Delta Project for CH_2Cl_2).

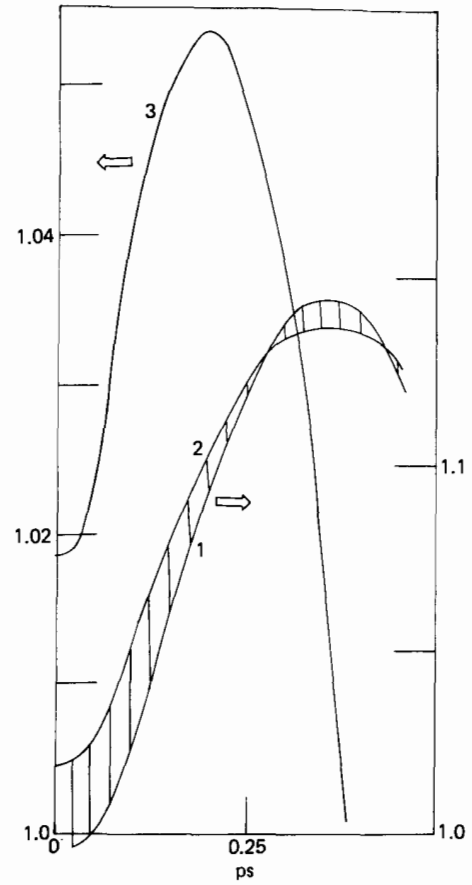

FIGURE 2.3.2.7. Some mixed energy a.c.f. components for CH_3CN. Curve 1: $\langle 1,1\rangle$; curve 2: $\langle 2,2\rangle$; curve 3: $\langle 3,3\rangle$.

To treat the *evolution of friction into memory*, equation (2.3.3.2) is readily written down when the friction coefficient is replaced by a memory function. It is convenient to start with the original generalized Langevin equation of Mori (1965). This is written for the center-of-mass linear velocity as

$$\dot{\vec{v}}(t) = -\int_0^t \phi(t-\tau)\vec{v}(\tau)\,d\tau + \vec{f}(t) \qquad (2.3.3.3)$$

This is a linear integrodifferential equation and is derived from the relevant Liouville equation by using projection operators. The memory kernel $\phi(t-\tau)$ may be expanded in a Mori continued fraction. Grigolini has shown, using Dupuis's algebraic methods, that this expansion may be taken effectively to infinity by introducing phenomenological parameters.

Grigolini and Marin (1981) have shown that the rotational equivalent to equation (2.3.3.3), namely

$$\dot{\vec{\omega}}(t) = -\int_0^t \Phi(t-\tau)\vec{\omega}(\tau)\,d\tau + \vec{f}(t) \tag{2.3.3.4}$$

may be treated in a similar manner. The continued-fraction expansion may again be taken to infinity. The above system of equations (2.3.3.1) is inherently nonlinear. This is due to the kinematic equation

$$\dot{\vec{u}} = \vec{\omega} \times \vec{u}$$

Expansion of either equation (2.3.3.3) or (2.3.3.4) in a Mori continued fraction is equivalent (Grigolini and Marin, 1981) to rewriting them as multidimensional linear equations of the type

$$\dot{\mathbf{A}} = \Gamma\mathbf{A} + \mathbf{F} \tag{2.3.3.5}$$

The column vector **A** may incorporate subvectors to take account of the effects of rotation and translation if there are no memory effects:

$$\mathbf{A} = \begin{bmatrix} \vec{\mathbf{v}} \\ \vec{\omega} \end{bmatrix} \tag{2.3.3.6}$$

That is,

$$\mathbf{A} = \begin{bmatrix} \begin{bmatrix} \vec{v}_0 \\ \vec{v}_1 \\ \vdots \\ \vec{v}_n \end{bmatrix} \\ \begin{bmatrix} \vec{\omega}_0 \\ \vec{\omega}_1 \\ \vdots \\ \vec{\omega}_n \end{bmatrix} \end{bmatrix} \tag{2.3.3.7}$$

The general idea of expanding $\mathbf{v}$ as $(\vec{v}_0, \vec{v}_1, \ldots, \vec{v}_n)$ is illustrated schematically in Fig. 2.3.3.1. For example, if $\mathbf{v}$ is identified with the particle executing Brownian motion, its motion is represented by the chain of variables $(\vec{v}_0, \ldots, \vec{v}_n)$. This is equivalent to the scheme shown in Fig. 2.3.3.1. Only the last (virtual) particle of the chain undergoes a motion that is influenced in a random fashion by the heat bath.

The chain of virtual particles having the effective velocities $(\vec{v}_0, \ldots, \vec{v}_n)$ and angular velocities $(\vec{\omega}_0, \ldots, \vec{\omega}_n)$ may be extended to large n. This is done by using the algebraic methods developed by Dupuis (1967) for computing continued fractions. The number n is in the range 10–100, depending on the

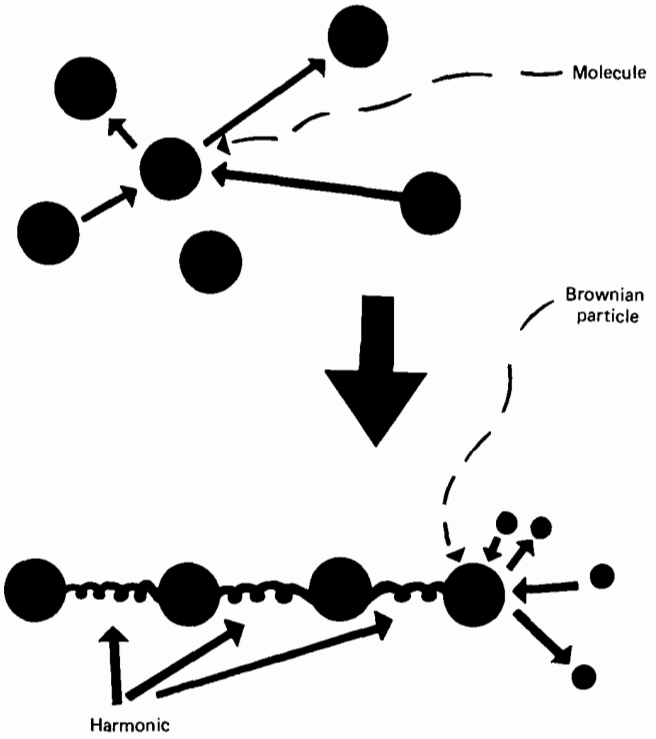

FIGURE 2.3.3.1. Brownian particle in a heat bath.

problem. The numerical solution converges to the solution of the Liouville equation for the complete system under consideration.

Our discussion pertains to the laboratory (i.e., fixed) frame of reference. In this frame, equation (2.3.3.5) decouples into purely rotational and translational parts in an analogous fashion to equation (2.3.3.1). In order to describe the effects observed in Section 2.2, we must rewrite equation (2.3.3.5) and solve it for rotation and translation in a moving frame of reference.

We can calculate an angular-velocity or linear-velocity a.c.f. in the moving frame by solving equation (2.3.3.5) in the moving frame of reference. We define a set of parameters $\zeta^{(t)}, \zeta^{(r)}, \zeta^{(tr)}, \zeta^{(rt)}$. These represent the interaction of the last virtual particle n with the rest of the heat bath. A description of the observed spectra, with full memory effects, is therefore possible by transforming this autocorrelation function into the laboratory frame.

2.3.4. Nonlinear Effects

Equations 2.3.3.3 and 2.3.3.4 are linear integrodifferential equations. The equation of motion of a molecule is in general of the form

$$\dot{\vec{v}} = -\frac{\partial V}{\partial \vec{r}} - \zeta\vec{v} + \vec{F}(t) \tag{2.3.4.1}$$

V is the potential energy and ζ a laboratory-frame friction coefficient. This reduces (Grigolini and Marin, 1981) to an equation having the form of equation (2.3.3.3) at short times. At long times it takes the form

$$\frac{d\vec{v}}{dt} = a(\vec{v}) + \vec{F}(t) \qquad (2.3.4.2)$$

In principle it is possible to determine the form of the interaction potential. This is done by using the results of Section 2.2. We transform equation (2.3.4.1) into the moving frame of reference.

2.4. SUGGESTIONS FOR FURTHER WORK

The suggested analytical approach of Section 2.3 will be effective only if sufficient information is available from computer simulation. This is needed to evaluate accurately the phenomenological variables required to describe the rotation observable in the moving frame of reference. For an effective simulation technique we need more accurate estimates of the pair interaction potential between molecules. One can do this readily by measuring the second dielectric virial coefficient B_ϵ over a wide range of conditions as mentioned above (Sutter, 1972).

A theoretical analysis of the moving-frame computer results could then be directed towards producing the phenomenological coefficients of Section 2.3. Having defined these coefficients, the theory could then produce a wide range of spectral results for coordinated experimental comparison. This would be done within the Delta Project framework.

A more complete link between analytical and computer simulation techniques is possible using the same form for the interaction potential V in both cases. This would maximize the coordination between the phenomenological equation (2.3.4.1) and the "kinetic theory" embodied in computer-simulation algorithms. We can arrive at an empirical correlation between the phenomenological coefficients, for example $\gamma^{(t)}$, $\gamma^{(r)}$, $\gamma^{(tr)}$, and $\gamma^{(rt)}$, for each molecule and its geometrical properties (e.g. moment-of-inertia ratio). We would like to describe the role of rotation and translation in the spectrum of liquid crystals. This could be done by studying the dynamics of increasingly elongated molecules. Tables of γ or ζ coefficients could be drawn up for different symmetries or geometries. A spectrum such as that in the zero-to-terahertz region (microwave and far infrared) would be described using approximately 100 memory functions. The FORTRAN algorithm necessary to do this would have as input tabulated ζ parameters, the friction coefficients of, say, the 101st memory function. The algorithm would be made iterative. Thus the spectrum under consideration could be matched closely by iterating on, or tuning, the ζ parameters. In principle, this procedure is the same as that of fitting a dielectric-loss spectrum to a given set of parameters.

ACKNOWLEDGMENT

The Science and Engineering Research Council (U.K.) is thanked for its generous financial support throughout the course of the project described here.

APPENDIX A: TAYLOR SERIES EXPANSION OF THE MIXED A.C.F.'S

The mixed a.c.f.'s $\langle\ \rangle_m$ in the moving frame are autocorrelation functions. Therefore, they do not change their form if we replace t by $-t$. This means that the time expansion of $\langle v_1(t)J_2(0)\rangle_{\text{mol}}$, say, contains even terms only, so that:

$$\begin{aligned}\langle v_1(t)J_2(0)\rangle_{\text{mol}} = &\left|\left[\langle v_1(t)J_2(0)\rangle_m\right]\right|_{t\to 0} \\ &+ \left|\frac{d^2}{dt^2}\left[\langle v_1(t)J_2(0)\rangle_m\right]\right|_{t\to 0}\frac{t^2}{2!} \\ &+ \left|\frac{d^4}{dt^4}\left[\langle v_1(t)J_2(0)\rangle_m\right]\right|_{t\to 0}\frac{t^4}{4!} + \cdots \qquad (A.1)\end{aligned}$$

We know that $[\langle v_1(t)J_2(0)\rangle_m]_{t\to 0} = 0$, but other coefficients are nonzero. In the laboratory frame, the coefficients vanish. It is possible to construct sum rules by evaluating these coefficients in the molecule frame of reference. It is evident that the a.c.f.'s in Section 2.2 start off with zero slope near $t = 0$. They therefore obey the fundamental equation (A.1).

APPENDIX B: FRAME CHANGES IN ROTATION–TRANSLATION COUPLING

If we denote the principal inertial (molecule-fixed) frame by (A, B, C) and the laboratory frame by (x, y, z), we have ($\vec{v}$ = linear, $\vec{\omega}$ = angular, velocity)

$$v_A = v_x e_{Ax} + v_y e_{Ay} + v_z e_{Az} \qquad (B.1)$$

$$v_B = v_x e_{Bx} + v_y e_{By} + v_z e_{Bz} \qquad (B.2)$$

$$v_C = v_x e_{Cx} + v_y e_{Cy} + v_z e_{Cz} \qquad (B.3)$$

$$\omega_A = \omega_x e_{Ax} + \omega_y e_{Ay} + \omega_z e_{Az} \qquad (B.4)$$

$$\omega_B = \omega_x e_{Bx} + \omega_y e_{By} + \omega_z e_{Bz} \qquad (B.5)$$

$$\omega_C = \omega_x e_{Cx} + \omega_y e_{Cy} + \omega_z e_{Cz} \qquad (B.6)$$

Because $\vec{e}_A$, $\vec{e}_B$, and $\vec{e}_C$ are unit vectors:

$$e_{Ax}^2 + e_{Ay}^2 + e_{Az}^2 = 1 \tag{B.7}$$

$$e_{Bx}^2 + e_{By}^2 + e_{Bz}^2 = 1 \tag{B.8}$$

$$e_{Cx}^2 + e_{Cy}^2 + e_{Cz}^2 = 1 \tag{B.9}$$

Transforming back into the laboratory frame, we get

$$v_x = v_A e_{Ax} + v_B e_{Bx} + v_C e_{Cx} \tag{B.10}$$

$$v_y = v_A e_{Ay} + v_B e_{By} + v_C e_{Cy} \tag{B.11}$$

$$v_z = v_A e_{Az} + v_B e_{Bz} + v_C e_{Cz} \tag{B.12}$$

Similarly, for the laboratory frame components of $\vec{\omega}$,

$$\omega_x = \omega_A e_{Ax} + \omega_B e_{Bx} + \omega_C e_{Cx} \tag{B.13}$$

$$\omega_y = \omega_B e_{Ay} + \omega_B e_{By} + \omega_C e_{Cy} \tag{B.14}$$

$$\omega_z = \omega_C e_{Az} + \omega_B e_{Bz} + \omega_C e_{Cz} \tag{B.15}$$

These fifteen equations are general and provide us with a whole series of extra relations with which to understand the rotational dynamics of a rigid, asymmetric rotator. If, for example, we substitute equation (B.1) into (B.10), equation (B.2) into (B.11), and equation (B.3) into (B.12), we obtain some extra constraints on unit vector components:

$$e_{Ax}^2 + e_{Bx}^2 + e_{Cx}^2 = 1 \tag{B.16}$$

$$e_{Ay}^2 + e_{By}^2 + e_{Cy}^2 = 1 \tag{B.17}$$

$$e_{Az}^2 + e_{Bz}^2 + e_{Cz}^2 = 1 \tag{B.18}$$

$$e_{Ax}e_{Ay} + e_{Bx}e_{By} + e_{Cx}e_{Cy} = 0 \tag{B.19}$$

$$e_{Ax}e_{Az} + e_{Bx}e_{Bz} + e_{Cx}e_{Cz} = 0 \tag{B.20}$$

$$e_{Ay}e_{Az} + e_{By}e_{Bz} + e_{Cy}e_{Cz} = 0 \tag{B.21}$$

The magnitude of the vectors $\vec{v}$ and $\vec{\omega}$ does not change on going from one frame to another. Thus

$$v_A^2 + v_B^2 + v_C^2 = v_x^2 + v_y^2 + v_z^2 \tag{B.22}$$

$$\omega_A^2 + \omega_B^2 + \omega_C^2 = \omega_x^2 + \omega_y^2 + \omega_z^2 \tag{B.23}$$

From the point of view of rotation–translation coupling we have the following general results on the basis of symmetry arguments alone:

$$\langle \mathbf{v}(t)\boldsymbol{\omega}^T(0)\rangle_{\text{lab}} = 0, \qquad \text{all } t \tag{B.24}$$

$$\langle \mathbf{v}(0)\boldsymbol{\omega}^T(0)\rangle_{\text{mol}} = 0, \qquad t = 0 \tag{B.25}$$

$$\langle \mathbf{v}(t)\boldsymbol{\omega}^T(0)\rangle_{\text{mol}} \neq 0 \qquad \text{in general for } t > 0 \tag{B.26}$$

In the specific case of CH_2Cl_2 the C_{2v} symmetry ensures that all the elements of the correlation matrix, equation (B.26), vanish except the $[A, B]$ and $[B, A]$ elements, i.e.

$$\langle v_A(t)\omega_B(0)\rangle \neq \langle v_B(t)\omega_A(0)\rangle \neq 0 \tag{B.27}$$

Using equations (B.1) and (B.5), we have

$$\langle \left[v_x(t)e_{Ax}(t) + v_y(t)e_{Ay}(t) + v_z(t)e_{Az}(t)\right] \times \left[\omega_x(0)e_{Bx}(0) + \omega_y(0)e_{By}(0) + \omega_z(0)e_{Bz}(0)\right]\rangle \tag{B.28}$$

In general, for a low-symmetry (e.g., optically active) molecule, there are 81 autocorrelation functions such as

$$\langle v_x(t)e_{Ax}(t)\omega_x(0)e_{Bx}(0)\rangle$$

which can be used in the laboratory frame to characterize rotation–translation coupling.

Lastly we point out that by using equations (B.1)–(B.9), for example, it is possible to express autocorrelation functions such as $\langle \omega_x(t)\omega_x(0)\rangle$ in terms of linear-velocity and angular-velocity components in the laboratory or molecule fixed frame. This is done by eliminating the nine components of $\vec{e}_A$, $\vec{e}_B$, and $\vec{e}_C$ via the nine equations.

Generally, therefore, the angular-velocity a.c.f. $\langle \vec{\omega}(t) \cdot \vec{\omega}(0)\rangle$ of the asymmetric diffuser contains elements of *linear* velocity in its makeup. By the kinematic relation $\dot{\vec{u}} = \vec{\omega} \times \vec{u}$, so do the rotational velocity a.c.f. $\langle \dot{\vec{u}}(t) \cdot \dot{\vec{u}}(0)\rangle$ of far-infrared spectroscopy and the orientational a.c.f. $\langle \vec{u}(t) \cdot \vec{u}(0)\rangle$ of dielec-

tric spectroscopy, infrared spectroscopy, and so on. Therefore, purely rotational theories of these spectra are greatly oversimplified.

REFERENCES

Ailawadi, N. K., Berne, B. J., and Foster, D., *Phys. Rev. A*, **3**, 1462 (1981).

Bellemans, A., Ciccotti, G., and Ryckaert, J.-P., *Mol. Phys.* **44**, 979 (1981).

Berne, B. J. and Harp, G. D., *Adv. Chem. Phys.* **17**, 203 (1970).

Berne, B. J. and Pecora, R., *Dynamic Light Scattering, with Reference to Physics, Chemistry and Biology*, Wiley-Interscience, New York, (1976).

Brier, P. and Perry, A., *Adv. Mol. Rel. Int. Proc.* **13**, 1–46 (1977).

Cheung, P. S. Y., *Mol. Phys.* **33**, 519 (1978).

Coffey, W. T. and Calderwood, J. H., *Proc. R. Soc. Lond. A* **356**, 269 (1977).

Condiff, D. W. and Dahler, J. S., *J. Chem. Phys.* **44**, 3988 (1966).

del Re, R., *J. Chem. Soc.* **36**, 161 (1958).

Deutch, J. M. and Wolynes, P. G., *J. Chem. Phys.* **67**, 733 (1977).

Dupuis, M., *Prog. Theoret. Phys.* **37**, 502 (1967).

Evans, G. T., *Mol. Phys.* **36**, 1199 (1978).

Evans, M. W. and Yarwood, J., *Adv. Mol. Rel. Int. Proc.* **21**, 2–87 (1981).

Evans, M. W., Evans, G. J., Coffey, W. T., and Grigolini, P., *Molecular Dynamics and Theory of Broad Band Spectroscopy*, Wiley-Interscience, New York (1982).

Ferrario, M., unpublished work.

Finney, J., *Disc. Faraday Soc., Canterbury* p. 80 and 86 (1978).

Goldstein, H., *Classical Mechanics*, Addison-Wesley, New York (1950).

Grigolini, P., and Marin, P., paper presented at EUCMOS, Session 15 EMLG; *J. Mol. Structure*, in press (1981).

Hill, N. E., Price, A. H., Vaughan, W. E., and Davies, M., *Dielectric Properties and Molecular Behaviour*, van Nostrand Reinhold, London (1968).

Hirschfelder, J. O., Curtiss, C. F., and Bird, R. B., *Molecular Theory of Gases and Liquids*, Wiley, New York (1964).

Hwang, L.-P. and Freed, J. H., *J. Chem. Phys.* **63**, 118, 4017 (1975).

Kielich, S., *Dielectric and Related Molecular Processes*, Vol. 1, M. Davies, Ed., The Chemical Society, London (1972).

McConnell, J. R., *Rotational Brownian Motion and Dielectric Theory*, Academic Press, London (1980).

Mori, H., *Prog. Theoret. Phys.* **33**, 423 (1965); **34**, 399 (1966).

Quentrec, B. and Brot, C., *Phys. Rev.* **12**, A272 (1975).

Reid, C. J. and Evans, M. W., *Mol. Phys.* **40**, 1357 (1980).

Scaife, B. K. P., *Complex Permittivity*, The English Universities Press, London (1971).

Scaife, B. K. P., *Proc. Phys. Soc.* **84**, 616 (1964).

Sutter, H., *Dielectric and Related Molecular Processes*, Vol. 1, M. Davies Ed., The Chemical Society, London (1972).

van der Avoird, A., Wormer, P. E. S., Mulder, F., and Berns, R. M., *Topics in Current Chemistry* Vol. 93, M. J. S. Dewar et al., Eds., Springer, 1980.

CHAPTER THREE

Models for the Effect of Dipole–Dipole Coupling on Dielectric Relaxation at Low Frequencies

3.1. THE DEBYE THEORY

We commence this chapter by reviewing very briefly the classical theory, due to Debye (1929), of dielectric relaxation of an assembly of dipolar molecules, the molecules of the assembly being supposed not to interact electrically with each other.

Debye considered a model where the dipoles are free to rotate in space. More specifically, each dipole is supposed to be fixed in a rigid sphere which is free to rotate in space, the sphere being subjected both to random white noise couples about its axis of rotation, having no preferential direction, and to the action of a time-varying field applied in a fixed direction. The distribution function f for the problem is defined as follows: $f\,d\Omega$ is the number of dipoles whose axes point into an element of solid angle $d\Omega$; thus f is a function both of the time and the angle ϑ between the axis of a dipole and the applied field. The average torque on an individual dipole due to its surroundings is $\zeta\dot{\vartheta}$. It is implicitly assumed that the inertia of the dipoles may be neglected and further that the electrical dipole–dipole coupling between them may also be ignored, so that *on the average* each dipole behaves in the *same* way. Thus, with the aid of the Smoluchowski equation (Evans et al., 1982), we find that $f(\vartheta, t)$ satisfies the equation

$$\frac{\partial f(\vartheta,t)}{\partial t} = \frac{1}{\sin\vartheta}\frac{\partial}{\partial\vartheta}\left[\sin\vartheta\left(\frac{kT}{\zeta}\frac{\partial f(\vartheta,t)}{\partial\vartheta} + \frac{\mu E}{\zeta}\sin\vartheta f(\vartheta,t)\right)\right] \tag{3.1.1}$$

which is simply the normal Smoluchowski equation written in spherical polar